

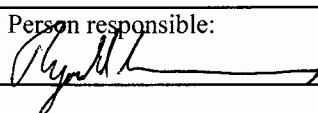
GEOLOGI FOR SAMFUNNET

GEOLOGY FOR SOCIETY



NGU Report 2012.036

Mannen unstable rock slope (Møre og Romsdal):
Geological and engineering geological logging of
drill core KH-02-11 & grain size distribution and
XRD analysis of fine-grained breccia

Report no.: 2012.036		ISSN 0800-3416	Grading: Open
Title: Mannen unstable rock slope (Møre og Romsdal): Geological and engineering geological logging of drill core KH-02-11 & grain size distribution and XRD analysis of fine-grained breccia			
Authors: T. Oppikofer, H. Bunkholt, G.V. Ganerød, A.K. Engvik		Client: Åknes/Tafjord Beredskap IKS	
County: Møre og Romsdal		Commune: Rauma	
Map-sheet name (M=1:250.000) Ålesund		Map-sheet no. and -name (M=1:50.000) 1319 II Romsdalen	
Deposit name and grid-reference: Mannen		Number of pages: 47	Price (NOK): 175
		Map enclosures: 0	
Fieldwork carried out: February 2012	Date of report: 28.11.2012	Project no.: 336700	Person responsible: 
Summary: Mannen is an unstable rock slope in the Romsdal Valley in the Møre og Romsdal County (western Norway). The slope is under continuous monitoring since 2009 by the Åknes/Tafjord Beredskap IKS. As part of the detailed site investigations, two boreholes have been drilled in 2010 and 2011. This report presents the results from the geological and engineering geological core logging of the lower, second borehole drilled in 2011 (KH-02-11), which complements the logging of the upper, first borehole (KH-01-10) and the geophysical borehole logging using an optical televiewer reported earlier. Results from grain size distribution of fine-grained breccias, as well as XRD identification of clay minerals in breccia layers for both boreholes at Mannen (KH-01-10 and KH-02-11) are also presented here. The drill core from borehole KH-02-11 is composed of the same lithologies as the upper borehole, but these could not be correlated between the boreholes, except possibly a 4 m thick pegmatite layer. The analysed drill core displays numerous severely fractured and crushed zones and zones with poor to very poor rock mass quality. Core diking is observed in the lower part of the borehole (96–131.6 m depth), which is generally an indicator of high horizontal in-situ stress. High fracture frequency and poor rock mass quality in parts affected by core diking are likely not representative for the in-situ rock mass. Fine-grained clayey breccias are observed in several of the crushed zones, notably at 66.28–66.76 m, 84.80 and 95.58 m depth. The breccias are characterized as mature, matrix-supported breccias based on the grain size distribution and also contain clay minerals (chlorite and illite in general, smectite at 66.70 m depth where a possible basal sliding surface is located). The fine-grained clayey breccias sampled in borehole KH-01-10 are also classified as mature, matrix-supported breccias at 27.90–28.61 m and 63.00 m depth, while the other samples are immature, grain-supported breccias. Most breccia samples from KH-01-10 contain chlorite. Illite and montmorillonite are found at 28 m depth in KH-01-10, where a possible basal sliding surface has previously been identified. These investigations and the optical televiewer logging of borehole KH-02-11 make it necessary to update the geological model. It is therefore recommended to combine these observations with other data from previous reports and with displacement measurements to establish a coherent geological model of the Mannen unstable rock slope.			
Keywords:	Geological core logging	Engineering geological core logging	
Fracture density	Rock Quality Designation	Sliding surface	
Grain size distribution	XRD characterization of clay minerals	Unstable rock slope	

CONTENTS

1. Introduction	5
2. Geological core logging.....	6
2.1 Description of lithologies	6
2.1.1 NGU sample #67359 (51.66 m depth): Sillimanite-bearing augengneiss	6
2.1.2 NGU sample #67360 (54.37 m depth): Sillimanite-bearing augengneiss	7
2.1.3 NGU sample #67361 (84.51 m depth): Muscovite-rich gneiss	8
2.1.4 NGU sample #67362 (88.95 m depth): Pegmatite.....	8
2.1.5 NGU sample #67363 (106.41 m depth): Amphibolitic gneiss	8
2.2 Summary of observations	8
3. Fracturing, crushed zones and fault rocks	10
4. Grain size distributions and XRD analyses of fine-grained breccia intervals.....	14
4.1 Methods	14
4.1.1 Grain size distribution.....	14
4.1.2 XRD analysis	14
4.2 Results	15
4.2.1 Grain size distribution.....	15
4.2.2 XRD analysis	17
5. Conclusions & recommendations.....	19
6. References	20

FIGURES

Figure 1: Map of the Mannen unstable rock slope in Romsdalen (Møre og Romsdal County, western Norway) with the extent of the unstable rock slope (three scenarios A, B and C) and the location of the boreholes KH-01-10 and KH-02-11. Topographic map from Statens Kartverk (1:50 000 scale).....	5
Figure 2: Microscope photographs of the thin-sections of rock samples from KH-02-11: a) sillimanite-bearing augengneiss (NGU sample # 67359) large K-feldspar porphyroblast within fine-grained matrix (image width: 2.7 mm); b) as in a) but with crossed nicols; c) fibrolite aggregate within sillimanite-bearing augengneiss (NGU sample # 67359, image width: 2.7 mm); d) sillimanite-bearing augengneiss (NGU sample # 67360) with foliation defined by oriented mica (image width: 5.3 mm); e) muscovite-rich gneiss (NGU sample # 67361) with coarse mica grains within medium-grained matrix (image width: 1.4 mm); f) medium-grained amphibolitic gneiss (NGU sample # 67363) with amphibole grains (image width: 2.7 mm). ..	7
Figure 3: Example photographs of fractured zones in borehole KH-02-11 (downward direction is to the right): a) fractured zone (at 24.8 m depth); b) crushed zone (at 25.2 m depth); c) brecciated zone (at 66.6 m depth); d) core dinking delaminating the drill core into small disks (at 122.3 m depth).	10
Figure 4: Grain size distributions from the breccia samples from a) borehole KH-01-10 and b) borehole KH-02-11. Samples from the same larger intervals with poor rock mass quality are plotted with the same colour. The limits between the matrix-supported, transitional and grain-supported domains from Henderson et al. (2010) are shown as dashed black lines.....	16

TABLES

Table 1: Rock samples for thin-section analyses.	6
Table 2: Summary of lithological observations along the drill core of borehole KH-02-11.	9
Table 3: Fracture frequency along the drill core of KH-02-11, thickness of fractured, crushed or brecciated zones and RQD values. The bars are proportional to the maximum number of 18 fractures respectively to 100 for the RQD.	11
Table 4: Large intervals of poor or very poor rock mass quality.	13
Table 5: Samples for XRD analysis and grain size distribution.	14
Table 6: Summary of the grain size distribution analysis of the fine-grained breccia samples including the mean grain diameter and the diameter at the 10 th , 50 th and 90 th percentiles (d10, d50 and d90, respectively), classification, distribution form and maturity of the breccia.	15
Table 7: Summary of the XRD analysis of the fine-grained breccia samples with the identified possible main minerals, likely minerals and other possible minerals. Minerals of the clay group are underlined.	18

APPENDIXES

- Appendix 1: Pictures of the drill core of borehole KH-02-11 with observations of the geological and engineering geological core logging.
- Appendix 2: Detailed description of the geological core logging of borehole KH-02-11.

1. INTRODUCTION

Mannen is a large unstable rock slope located on the south-western flank of Romsdalen in the county of Møre og Romsdal (western Norway). The site has been investigated in detail by the Geological Survey of Norway (NGU) with geological field mapping, displacement measurements by differential Global Navigation Satellite Systems (dGNSS or dGPS) and terrestrial laser scanning, analysis of digital elevation models, electric resistivity profile, volume estimations, numerical stability modelling, run-out analyses and risk assessment (Henderson and Saintot 2007, Dahle et al. 2008, Dahle et al. 2011a, Dahle et al. 2011b, Farsund 2011, Saintot et al. 2011, Dalsegg and Rønning 2012). Since 2009 the unstable rock slope at Mannen is under continuous monitoring coupled to an early-warning system operated by the Åknes/Tafjord Early-Warning Centre in Stranda, Norway (Kristensen and Blikra 2011).

Two cored boreholes were made in 2010 and 2011 as part of the additional site investigations and the displacement monitoring system. NGU was mandated by the Åknes/Tafjord Early-Warning Centre for the geological and engineering geological logging of the drill cores and for geophysical logging of the boreholes using an optical televiewer. Results from the 138m-deep upper borehole (KH-01-10) are reported by Saintot et al. (2011), while results from the televiewer logging of the 132m-deep lower borehole (KH-02-11) are reported by Elvebakk (2012). Here we report on the geological and engineering geological logging of the drill cores of the lower borehole (KH-02-11). Results on the grain size distribution and mineralogical composition (XRD analysis) of clay-rich intervals encountered in both drill cores are also reported here, since the results for KH-01-10 were not available in time for being included in previous reports on the upper borehole (Saintot et al. 2011).

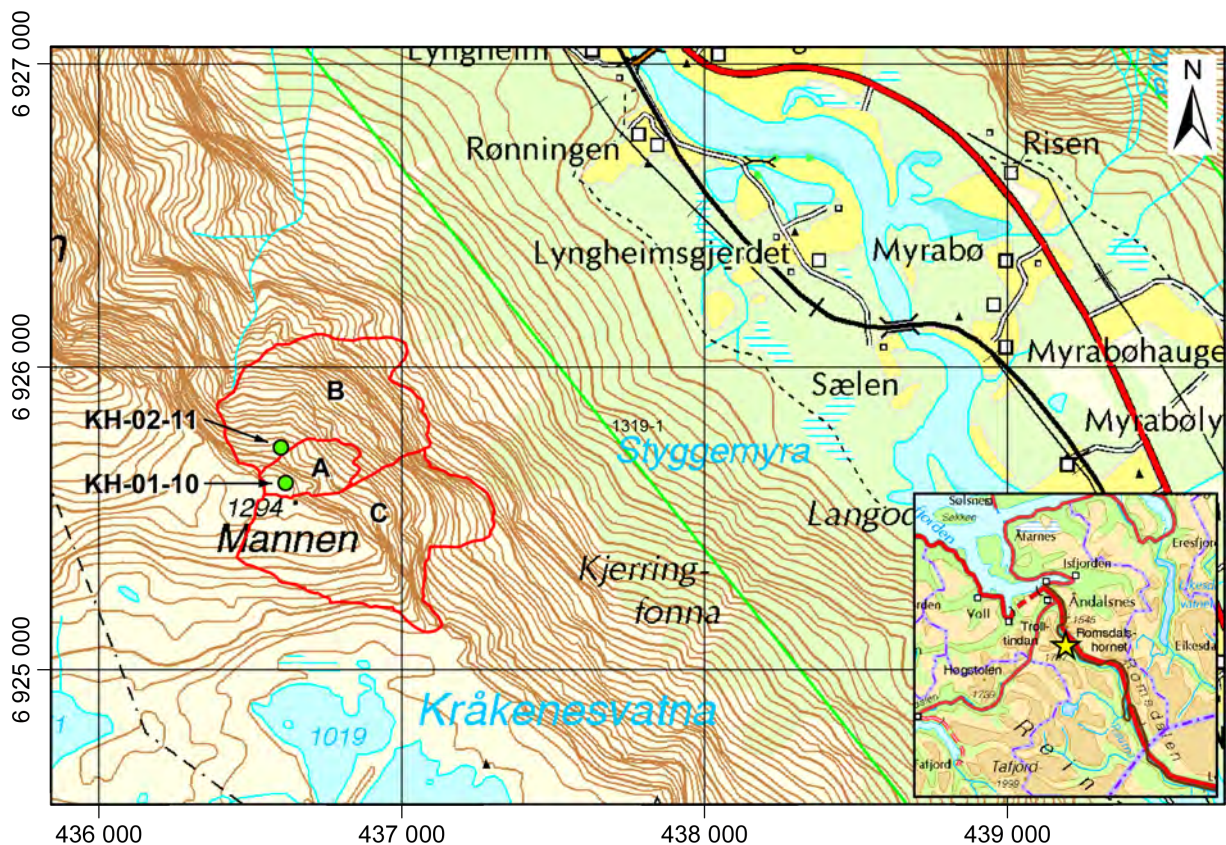


Figure 1: Map of the Mannen unstable rock slope in Romsdalen (Møre og Romsdal County, western Norway) with the extent of the unstable rock slope (three scenarios A, B and C) and the location of the boreholes KH-01-10 and KH-02-11. Topographic map from Statens Kartverk (1:50 000 scale).

2. GEOLOGICAL CORE LOGGING

The drill core of borehole KH-02-11 from the Mannen unstable rock slope was logged on 21 and 22 February 2012 at the Åknes/Taffjord Early-Warning Centre in Stranda. The geological logging focused on the different lithologies and their sequence in the borehole. The depths reported herein refer to the depths indicated on the core boxes. However, comparison with the optical televiewer logging of the borehole KH-02-11 (Elvebakk 2012) shows a variable shift of 0 to +60 cm between the depths on the core boxes and the televiewer depths, which can be considered as precise. In average the depths marked on the core boxes are ca. 30 cm higher than the televiewer depths. This discrepancy is explained by the presence of heavily fractured, crushed zones and core loss.

2.1 Description of lithologies

The lithologies encountered in borehole KH-02-11 are similar to those in borehole KH-01-10 (Saintot et al. 2011) in the form of fine- to medium-grained gneisses and augengneisses with well developed foliation. Other lithologies are pegmatites and amphibolitic gneisses. Saintot et al. (2011) have divided the encountered rocks into six types, which were also adopted for the present report:

- 1) Pegmatite
- 2) Amphibolite or amphibolitic gneiss
- 3) Fine-grained strongly foliated garnet- and sillimanite-bearing gneiss
- 4) Fine-grained strongly foliated garnet- and sillimanite-bearing augengneiss
- 5) Medium- to coarse-grained garnet-, sillimanite- and muscovite-bearing gneiss
- 6) Medium- to coarse-grained garnet-, sillimanite- and muscovite-bearing augengneiss

However, the observed lithologies not always fitted into one of these six rock types and other combinations are possible, for example coarse-grained gneisses without muscovite or fine-grained gneiss without well developed foliation.

For further characterization of the lithologies, samples for thin-section analyses were taken during the geological core logging of borehole KH-02-11 (Table 1).

Table 1: Rock samples for thin-section analyses.

NGU sample #	Borehole	Depth [m]	Material
67359	KH-02-11 (lower)	51.66	Sillimanite-bearing augengneiss
67360	KH-02-11 (lower)	54.37	Sillimanite-bearing augengneiss
67361	KH-02-11 (lower)	84.51	Muscovite-rich gneiss
67362	KH-02-11 (lower)	88.95	Pegmatite
67363	KH-02-11 (lower)	106.41	Amphibolitic gneiss

2.1.1 NGU sample #67359 (51.66 m depth): Sillimanite-bearing augengneiss

Main minerals: Quartz, K-feldspar, biotite, muscovite, sillimanite (mainly as fibrolite)

Minor minerals: Plagioclase, chlorite (maybe of secondary origin)

Accessory minerals: Zircon, opaque minerals

Texture & structure: Fine-grained with larger porphyroblasts of K-feldspar (Figure 2a, b), quartz and fibrolite aggregates (sillimanite) (Figure 2c). Foliation defined by the longitudinal direction of porphyroblasts and oriented mica. Weak gneiss banding with slight modal enrichment of mica in layers is observed. Feldspars are slightly sericitised.



Figure 2: Microscope photographs of the thin-sections of rock samples from KH-02-11: a) sillimanite-bearing augengneiss (NGU sample # 67359) large K-feldspar porphyroblast within fine-grained matrix (image width: 2.7 mm); b) as in a) but with crossed nicols; c) fibrolite aggregate within sillimanite-bearing augengneiss (NGU sample # 67359, image width: 2.7 mm); d) sillimanite-bearing augengneiss (NGU sample # 67360) with foliation defined by oriented mica (image width: 5.3 mm); e) muscovite-rich gneiss (NGU sample # 67361) with coarse mica grains within medium-grained matrix (image width: 1.4 mm); f) medium-grained amphibolitic gneiss (NGU sample # 67363) with amphibole grains (image width: 2.7 mm).

2.1.2 NGU sample #67360 (54.37 m depth): Sillimanite-bearing augengneiss

Main minerals: Quartz, K-feldspar, plagioclase, biotite, muscovite, sillimanite (mainly as fibrolite)

Accessory minerals: Opaque minerals, apatite, zircon

Texture & structure: Fine-grained with larger grains of quartz and fibrolite aggregates (sillimanite). Foliation defined by the longitudinal direction of oriented mica (Figure 2d), quartz aggregates and fibrolite. Gneiss banding with modal enrichment of mica in layers is observed. Feldspars are slightly sericitised.

2.1.3 NGU sample #67361 (84.51 m depth): Muscovite-rich gneiss

Main minerals: Plagioclase, K-feldspar, quartz, biotite, light-colored mica

Accessory minerals: Opaque minerals, zircon, apatite

Texture & structure: Medium-grained with relatively equal grain-size, but some coarse mica grains (Figure 2e). Foliation is defined by the longitudinal direction of oriented mica. Feldspars are slightly seriticised.

2.1.4 NGU sample #67362 (88.95 m depth): Pegmatite

Main minerals: Quartz, plagioclase, K-feldspar, light-colored mica

Minor mineral: Garnet

Accessory mineral: Apatite

Texture & structure: Coarse to very coarse grains of quartz and feldspars with sutured grain boundaries; fine- to medium-grained garnet. Slight longitudinal orientation of quartz grains along with oriented light-colored mica. Feldspars are seriticised.

2.1.5 NGU sample #67363 (106.41 m depth): Amphibolitic gneiss

Main minerals: Plagioclase, K-feldspar, quartz, amphibole, biotite

Minor minerals: Epidote, scapolite

Accessory minerals: Opaque minerals, apatite

Texture & structure: Medium-grained with relatively equal grain-size (Figure 2f). Foliation is defined by modal banding (enrichment of mafic minerals in layers) and oriented biotite. Feldspars are slightly seriticised.

2.2 Summary of observations

A summary of lithological observations along the drill core is presented in Table 2. More details can be found in the pictures of the drill core (Appendix 1) and the detailed table of the geological core logging observations (Appendix 2).

The cores of the lower borehole KH-02-11 show some striking differences with those of the upper borehole KH-01-10 in terms of degree of folding, orientation of foliation and sequence of lithologies:

- Numerous fold hinges were observed in the upper borehole, while these were relatively rare in the lower borehole. In both boreholes fold hinges were mainly visible in amphibolitic layers.
- Foliation is generally steeply-dipping to subvertical in the lower borehole, while it was moderately-dipping the upper borehole.
- The sequence of rock types encountered in the lower borehole is not comparable to the upper borehole. The only possible marker is the 4 m thick pegmatite layer, which is observed at 87–91 m depth in the lower borehole (see Figures A1.14 and A1.15) and at 43–47 m depth in the upper borehole. However, this pegmatite layer is surrounded by fine-grained strongly foliated gneiss in the lower borehole compared to augengneisses in the upper borehole, which indicates that the pegmatite is probably discordant to the foliation. Any further correlation is thus impossible.

Table 2: Summary of lithological observations along the drill core of borehole KH-02-11.

Depth [m]	Type	Description
0–6	-	Core loss
6–7	3	Fine-grained well foliated amphibole-rich gneiss
7–28	6, 4	Predominantly foliated augengneiss with variable grain size. Fine-grained matrix of amphibole and biotite with K-feldspar porphyroblasts (augens) showing ductile deformation. Locally plagioclase augens. The foliation is overall well developed, displaying varying dip. Locally felsic mineral infill in veins. Sillimanite appears in overall mafic associations, but disappear at core length 20.4 m. The bedrock is competent with few fractures.
28–44	2	Fine-grained well foliated amphibolitic gneiss displaying a strong shear deformation. Single minerals aggregates are elongated into thin foliation-parallel felsic bands. The mafic matrix is dominated by amphibolites and biotite. Locally, feldspar lenses are present. The felsic content is gradually reduced with depth in the interval. At 35.5–36.5 m a one meter thick pegmatite is observed. Towards 44 m there is a gradual transition to dominantly very dark bedrock. The last meter of the interval is crushed.
44–59	6	Well foliated augengneiss with K-feldspar augens of ~7–10 mm in size. The foliation is alternating between steeply dipping to vertical. Between 52.0–54.5 m there is a shift to lighter colors of the augens in a mafic matrix. Below this interval the lithology returns to being similar as at interval at 44–52 m depth. The shear varies somewhat throughout the interval. Typically the shear is displayed by minerals elongated into needle shape. Dependent on the viewed cut, these needle-shaped minerals display either an intersection lineation with the core side, or a dot intersection. Sigma clasts are common displaying varying rotation caused by shear.
59–62	3	Fine-grained gneiss with little or no K-feldspar porphyroblasts present. The bedrock is rich in muscovite. The foliation is well developed. Felsic veins are locally discordant to foliation.
62–66	5	This interval is similar to the interval between 59–62 m, but displays bands of recrystallized coarse-grained felsic minerals with a fine-grained mafic matrix.
66–67	2	Crushed zone within a ca. 1 m thick amphibolite layer, clay-rich breccia
67–76	3	Fine-grained gneiss with a high mafic content. Little porphyroblasts. The bedrock is overall highly strained. The foliation is well developed and displays high dip angles. Due to the fine grain size and lack of markers such as e.g. elongated minerals, local zones do however not display any detectable foliation in hand piece. A 50 cm thick pegmatite has intruded into the gneiss at 71.2–71.7 m depth. The fine-grained gneiss below that pegmatite intrusion displays high strain rates as seen by foliation parallel veins.
76–83	4, 6	Fine- to medium-grained augengneiss with predominantly K-feldspar augens, but locally also quartz and/or plagioclase augens. Local zones display abundant sillimanite. The interval is well foliated and competent with few fractures. Dextral shear is observed on indicators
83–87	3	Fine-grained strongly foliated gneiss with a high content of muscovite and biotite. Contains a fracture filled with fine-grained breccia at 84.85.
87–91	1	Pegmatite
91–102	3, 2	Fine-grained strongly foliated biotite-rich gneiss rich. Contains layers of amphibolites displaying a greenish color, probably due to retrograde chlorite alteration. Common minerals in hand piece are quartz, plagioclase, hornblende and biotite. There is an apparent separation in bands felsic and mafic minerals. Muscovite is concentrated in discrete zones. Dextral shear is displayed on indicators. Zones of vuggy rock occur and are commonly associated with chlorite-altered amphibolite layers. Scattered garnets are common.
102–104	4	Fine-grained strongly foliated augengneiss with K-feldspar augens. Some sillimanite are observed at 103.5 m.
104–126	3, 5	Fine-grained mafic gneiss of predominantly hornblende and scattered quartz of varying size. There are discrete zones displaying varying strain rates and locally dextral shear where indicators are observed. The foliation in the interval is well developed. Between 104–109 m quartz is almost not visible in macroscopic samples. The next 4 meters down to 113 m there is an increase in quartz content and grain size. In the remaining parts of the interval down to 125 m quartz minerals between 1–3 mm in size are scattered.
126–131.6	5, 6	Fine- to medium-grained strongly foliated gneiss with a high content of biotite and muscovite in discrete zones, which also define the foliation planes. The high mica content leads to an increased schistosity, on which delamination occur. Sillimanite-bearing augengneiss occurs in two zones. End of the core at 131.6 m depth.

3. FRACTURING, CRUSHED ZONES AND FAULT ROCKS

The geological and structural core logging of the lower borehole KH-02-11 at Mannen includes also a systematic logging of joints and fractures in the drill core, as well as the thickness of fractured, crushed or brecciated zones. In fractured zones the fracturation was too dense to count individual fractures (Figure 3a), while the fragments in crushed zones are generally smaller and cannot be reassembled as in fractured zones (Figure 3b). Brecciated zones are similar to crushed zones, but with even smaller fragments that form a fine-grained breccia (Figure 3c). These terms can thus be considered as indicators of increasing fracturation from fractured, crushed to brecciated.

The Rock Quality Designation (RQD) value (Deere 1964) was measured for each meter of the drill core (Table 3). The RQD is the total length of all drill core bits that are longer than 10 cm per meter of drill core. The RQD value thus ranges from 0 (completely crushed or heavily fractured rock mass) to 100 (nearly intact rock mass). Intervals with poor or very poor rock mass quality (RQD < 50 or RQD < 25, respectively) are mainly caused by a combination of high fracture frequency, fractured or even crushed zones and core loss (Table 4).

The core from borehole KH-02-11 is affected by the phenomena of core diskings between 96 and 131.6 m depth and especially down from 105 m depth. Core diskings delaminates the drill core into small disks with fractures perpendicular to the borehole axis (Figure 3d). Core diskings is generally an indicator of high horizontal in-situ stress (in a vertical borehole) (Jaeger and Cook 1963). These core diskings fractures induce a high fracture frequency in the extracted drill core, which is not representative for the fracture frequency of the in-situ rock mass. The fractures related to core diskings were therefore identified and separated from other fractures, where possible (Table 3). However, it was not possible to neglect these core diskings fractures in the assessment of the RQD. The measured RQD values are thus likely too low in zones affected by core diskings.

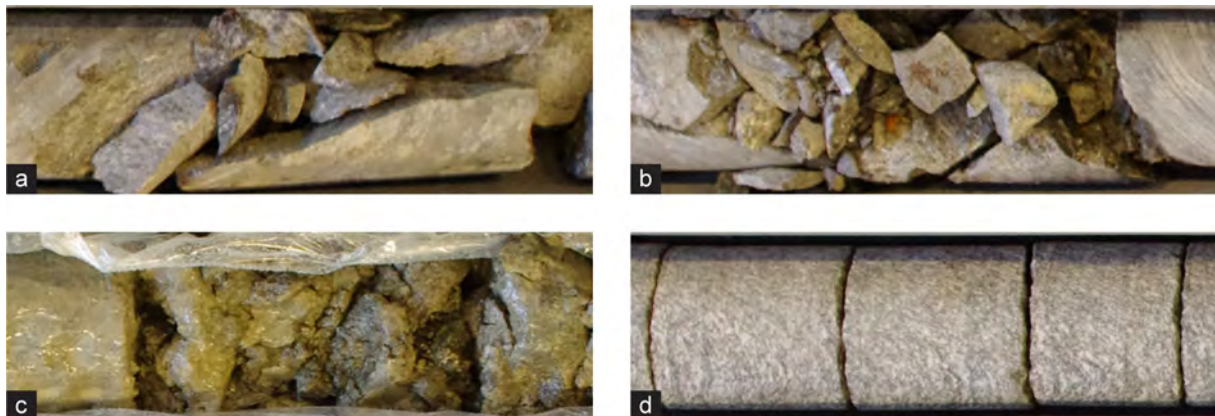


Figure 3: Example photographs of fractured zones in borehole KH-02-11 (downward direction is to the right): a) fractured zone (at 24.8 m depth); b) crushed zone (at 25.2 m depth); c) brecciated zone (at 66.6 m depth); d) core diskings delaminating the drill core into small disks (at 122.3 m depth).

Table 3: Fracture frequency along the drill core of KH-02-11, thickness of fractured, crushed or brecciated zones and RQD values. The bars are proportional to the maximum number of 18 fractures respectively to 100 for the RQD.

Depth [m]	Fracture frequency			Fractures due to core dinking	Thickness of fractured and crushed zones				RQD
	Total	Foliation	Other		Crushed [cm]	Fractured [cm]	Breccia [cm]	Core loss [cm]	
6-7	10	0	10	0	0	0	0	0	63
7-8	8	2	6	0	13	28	0	0	47
8-9	13	3	10	0	22	14	0	0	47
9-10	1	0	1	0	0	0	0	0	100
10-11	4	1	3	0	0	9	0	0	82
11-12	5	1	4	0	0	0	0	0	91
12-13	8	0	8	0	0	7	0	0	82
13-14	13	3	10	0	2	0	0	0	86
14-15	5	0	5	0	0	0	0	18	72
15-16	4	0	4	0	0	8	0	0	85
16-17	2	0	2	0	0	0	0	0	92
17-18	3	0	3	0	0	0	0	0	82
18-19	5	0	5	0	0	0	0	3	97
19-20	5	1	4	0	0	0	0	0	91
20-21	4	1	3	0	0	0	0	0	90
21-22	8	2	6	0	0	0	0	0	64
22-23	7	1	6	0	13	0	0	0	72
23-24	5	1	4	0	0	0	0	0	87
24-25	12	2	10	0	13	17	0	0	45
25-26	14	5	9	0	11	0	0.5	0	54
26-27	5	0	5	0	14	0	0	0	83
27-28	11	0	11	0	0	18	0	0	39
28-29	14	7	7	0	7	0	0	0	58
29-30	12	8	4	0	20	0	2	0	43
30-31	6	6	0	0	0	0	0	0	81
31-32	4	4	0	0	0	0	0	0	97
32-33	11	7	4	0	0	0	0	0	71
33-34	18	8	10	0	0	0	0	0	27
34-35	9	1	8	0	4	4	0	0	64
35-36	11	3	8	0	0	0	0	0	43
36-37	12	3	9	0	5	14	0	0	61
37-38	12	2	10	0	17	0	0	0	36
38-39	6	1	5	0	15	0	0	0	71
39-40	9	4	5	0	0	3	0	0	65
40-41	8	3	5	0	0	8	0	0	72
41-42	10	4	6	0	0	0	0	0	70
42-43	16	8	8	0	9	0	0	0	52
43-44	12	8	4	0	39	17	0	0	34
44-45	12	6	6	0	18	0	1	0	50
45-46	6	2	4	0	0	0	0	0	88
46-47	2	2	0	0	37	0	0	37	15
47-48	11	1	10	0	12	0	0	0	61
48-49	9	3	6	0	0	0	0.1	5	89
49-50	3	0	3	0	79	0	0	0	13
50-51	6	0	6	0	23	6	0	0	57
51-52	5	0	5	0	2	56	0	0	33
52-53	12	0	12	0	32	0	0	12	23
53-54	11	3	8	0	27	0	0	0	31
54-55	10	4	6	0	13	0	0	0	63
55-56	11	3	8	0	10	0	0	0	72
56-57	11	8	3	0	0	0	0	0	61
57-58	6	5	1	0	24	0	0	0	68
58-59	11	5	6	0	0	0	0	0	75
59-60	9	6	3	0	23	0	0.2	0	56
60-61	5	1	4	0	0	0	0	0	95
61-62	5	2	3	0	6	0	0	0	87
62-63	13	2	11	0	0	0	0	0	48
63-64	3	1	2	0	50	0	0	18	32
64-65	6	0	6	0	13	0	0	0	67
65-66	4	0	4	0	25	0	0	0	72
66-67	7	2	5	0	12	0	26	0	31
67-68	11	1	10	0	0	0	0	0	53
68-69	9	4	5	0	22	0	0	0	63

Table 3: (continued)

Depth [m]	Fracture frequency			Fractures due to core discing	Thickness of fractured and crushed zones				RQD
	Total	Foliation	Other		Crushed [cm]	Fractured [cm]	Breccia [cm]	Core loss [cm]	
69-70	7	2	5	0	0	17	0	0	74
70-71	12	5	7	0	3	0	0	0	48
71-72	7	1	6	0	53	0	0	0	37
72-73	6	1	5	0	0	0	0	0	89
73-74	6	1	5	0	29	0	0	0	63
74-75	6	5	1	0	0	0	0	0	81
75-76	14	6	8	0	5	0	0	0	59
76-77	10	2	8	0	8	0	0	0	71
77-78	10	2	8	0	0	0	0	0	73
78-79	8	2	6	0	0	0	0	0	87
79-80	6	2	4	0	0	0	0	0	82
80-81	10	6	4	0	0	0	0	0	49
81-82	11	8	3	0	40	0	0	0	22
82-83	10	3	7	0	0	0	0	0	77
83-84	12	6	6	0	21	0	0	25	0
84-85	17	11	6	0	32	4	11	0	0
85-86	18	10	8	0	0	0	0	5	31
86-87	6	6	0	0	2	0	0	0	83
87-88	10	0	10	0	5	0	0	0	57
88-89	4	0	4	0	2	0	0	0	88
89-90	2	0	2	0	0	0	0	3	97
90-91	8	6	2	0	0	0	0	0	84
91-92	17	8	9	0	19	0	0	0	25
92-93	6	3	3	0	0	22	0	0	47
93-94	13	7	6	0	0	4	0	0	53
94-95	12	6	6	0	21	0	0	3	54
95-96	5	4	1	0	41	22	2	0	35
96-97	3	1	2	1	0	42	0	0	54
97-98	10	6	4	0	0	0	0	0	52
98-99	8	3	5	0	4	0	0	0	64
99-100	8	1	7	2	23	0	0	0	26
100-101	13	4	9	0	4	0	0	0	41
101-102	6	1	5	0	0	0	0	0	86
102-103	8	2	6	0	0	0	0	0	75
103-104	5	1	4	0	0	34	0	0	64
104-105	13	3	10	0	0	0	0	0	41
105-106	9	3	6	4	0	0	0	0	48
106-107	3	2	1	6	9	0	0	0	64
107-108	2	1	1	4	0	0	0	0	84
108-109	5	2	3	2	0	52	0	0	24
109-110	6	1	5	3	30	0	0	0	38
110-111	5	1	4	3	0	0	0	0	80
111-112	6	1	5	3	0	0	0	0	71
112-113	6	3	3	0	9	0	0	0	88
113-114	5	1	4	0	0	0	0	0	79
114-115	9	3	6	0	0	0	0	7	71
115-116	10	2	8	0	4	0	0	0	69
116-117	4	1	3	5	5	0	0	0	48
117-118	6	0	6	4	27	0	0	0	19
118-119	5	0	5	0	0	63	0	0	10
119-120	0	0	0	0	0	100	0	0	0
120-121	8	2	6	3	0	19	0	0	42
121-122	1	1	0	9	0	0	0	0	54
122-123	3	0	3	8	4	0	0	0	39
123-124	9	3	6	3	0	0	0	0	58
124-125	7	2	5	9	12	3	0	0	26
125-126	6	4	2	12	10	0	0	0	11
126-127	7	2	5	1	6	50	0	0	25
127-128	6	4	2	10	14	7	0	0	21
128-129	8	6	2	3	0	0	3	0	61
129-130	5	2	3	14	31	0	0	0	0
130-131	4	3	1	2	11	21	0	43	13
131-131.6	0	0	0	0	0	60	0	0	0

Table 4: Large intervals of poor or very poor rock mass quality.

Depth [m]	Rock type	Description
24.50–26.14	3	Poor rock mass quality due to high fracture frequency and severely fractured and crushed zones (Figure A1.4). A 5 mm thick breccia is found at 25.32 m depth.
27.35–29.62	4, 2	Poor rock mass quality due to high fracture frequency and several severely fractured and crushed zones. A 2 cm thick layer with hard silty material is observed at the base of this zone at 29.62 m depth (Figure A1.4).
33.00–38.15	2, 1	Fair to poor rock mass quality due to high fracture frequency and few crushed zones. A 32 cm thick crushed zone is found at 37.73–38.15 m depth. At this level the borehole had to be stabilized before drilling continued (Figures A1.5, A1.6).
42.91–44.60	2, 6	Fair to poor rock mass quality due to high fracture frequency and several severely fractured and crushed zones (Figure A1.7).
46.26–47.12	6	Very poor rock mass quality due to crushed zones and core loss (Figure A1.7).
49.21–53.16	6	Poor to very poor rock mass quality due to multiple severely fractured and crushed zones and high fracture frequency, especially between 52.00–53.16 m depth (Figure A1.8). This interval with poor rock mass quality is located where the foliation dip angle decreases from subvertical to moderate.
63.16–66.76	5, 2	Fair to poor rock mass quality due to several crushed zones (Figures A1.10, A1.11). A 26 cm thick zone with fine-grained clayey breccia is found at 66.50–66.76 m depth within a moderately-dipping amphibolite layer. This breccia can be related to past displacements of the rock slide and might thus be the expression of the basal sliding surface.
70.30–72.00	3, 1	Poor rock mass quality due to high fracture frequency and several crushed zones. (Figure A1.11)
80.30–85.05	3, 6	Poor to very poor rock mass quality due to high fracture frequency and multiple severely fractured, crushed zones and core loss (Figures A1.13, A1.14). A 11 cm thick fine-grained clayey breccia is observed at 84.75–84.86 m depth within mica-rich gneiss with well developed moderately-dipping foliation.
91.05–96.42	3, 2	Fair to poor rock mass quality due to high fracture frequency and multiple severely fractured and crushed zones (Figures A1.15, A1.16). A 2 cm thick clayey breccia is found at 95.58–95.60 m depth within amphibolitic gneiss.
108.00–109.52	3	Poor to very poor rock mass quality due to core diskings leading to high fracture frequency and few crushed zones (Figure A1.18)
117.38–120.19	5	Poor to very poor rock mass quality due to core diskings leading to high fracture frequency and few crushed zones (Figures A1.19, A1.20)
124.34–131.60	5, 3, 6	Poor to very poor rock mass quality due to core diskings leading to high fracture frequency and few crushed zones (Figures A1.20, A1.21)

4. GRAIN SIZE DISTRIBUTIONS AND XRD ANALYSES OF FINE-GRAINED BRECCIA INTERVALS

Several intervals with fine-grained breccia (silty to clayey material) were observed during the core logging and sampled for XRD analysis of clay minerals and grain size distribution. Table 5 gives an overview of the samples taken in both boreholes, KH-01-10 and KH-02-11. Results from all samples are reported here since the data for borehole KH-01-10 were not ready in time for being included in previous reports (Saintot et al. 2011).

Table 5: Samples for XRD analysis and grain size distribution.

NGU sample #	Borehole	Depth [m]	Material
47285	KH-01-10 (upper)	27.91	Fine-grained breccia
47286	KH-01-10 (upper)	28.23	Fine-grained breccia
47287	KH-01-10 (upper)	28.58	Fine-grained breccia
47288	KH-01-10 (upper)	57.20	Fine-grained breccia
47289	KH-01-10 (upper)	63.00	Fine-grained breccia
47290	KH-01-10 (upper)	63.66	Fine-grained breccia
47291	KH-01-10 (upper)	67.60	Fine-grained breccia
67353	KH-02-11 (lower)	25.32	Fine-grained breccia
67354	KH-02-11 (lower)	66.30	Fine-grained breccia
67355	KH-02-11 (lower)	66.60	Fine-grained breccia
67356	KH-02-11 (lower)	66.70	Fine-grained breccia
67357	KH-02-11 (lower)	84.85	Fine-grained breccia
67358	KH-02-11 (lower)	95.58	Fine-grained breccia

4.1 Methods

4.1.1 Grain size distribution

The grain size distributions of the fine-grained breccia samples were analysed at NGU-Lab by gravimetric measurement (sieving) for grain size fractions $>2000 \mu\text{m}$ and by laser diffraction for grain size fractions between $0.4\text{--}2000 \mu\text{m}$ using a Coulter LS 200 instrument. The grain size fraction below $0.4 \mu\text{m}$ is not analysed. No sample preparation was required. The laser diffraction technique is based on the diffraction of laser light in different angles depending on the grain size of the encountered particles. The diffracted laser beams are then registered by a series of detectors. The registered angles match given particle sizes and the number of particles is related to the intensity that the corresponding detector registers. The grain size distribution is thus determined on volume basis, with the assumption of a material with homogeneous density where the cumulative volume percentage will be identical to the cumulative mass percentage. The uncertainty of the grain size distribution analysis on the cumulative mass (volume) percentage is given with $\pm 10 \%$ (2σ).

4.1.2 XRD analysis

The identification of clay minerals in the fine-grained breccia samples was performed at NGU-Lab using a Philips X'pert MPD with a Cu X-ray tube. The principle of X-ray diffraction (XRD) is based on the property that the reflection of a monochromatic X-ray beam emitted into a crystal surface is dependent on the crystal lattice structure. In practice is the X-ray beam emitted with varying incidence angles, θ , onto the sample and the reflections are recorded by a detector at the matching outcome angles (equal to θ). These angles, generally noted as 2θ , correspond to lattice spacings that are related to different crystal faces and are registered in the form of a diffractogram. Thus, each mineral gives a unique pattern of reflections on the diffractogram. Identification of minerals is then done by comparing

diffractograms of unknown samples with a database of patterns for known minerals. The samples are analysed with different pre-treatments: 1. air-dried, 2. glycolation by ethylene glycol, 3. heat treatment at 550°C for one hour. The samples are then analysed in the diffractometer with 2θ angles ranging from 1.5° to 69° for air-dried samples and from 2° to 35° for glycolated and heated samples. 0.04° 2θ was used as step size for all samples. Details can be found in the NGU-Lab analysis reports no. 2011.0039 and 2012.0060.

4.2 Results

4.2.1 Grain size distribution

The results from the grain size distribution of the breccia samples from Mannen are presented in Table 6 and Figure 4. The raw data are given in the NGU-Lab analysis reports no. 2011.0039 and 2012.0060.

Breccia samples can be classified according to the fault rock terminology proposed by Twiss and Moores (2007) based on the size of clasts:

- Breccia: clasts > 1 mm
- Microbreccia: clasts < 1 mm
- Gouge: clasts < 0.1 mm

Here, the diameter of the 90th percentile of the grain size distribution (d90) is used as size of clasts to classify the different breccia types. Most of the samples taken from the boreholes at Mannen are breccias with clast sizes above 1 mm, but three samples (#47285, 47286 and 67358) have smaller clast sizes and are therefore called microbreccias (Table 6).

The grain size distribution of breccia samples gives an indication about the textural maturity of the breccia (Henderson et al. 2010). Concave distributions are associated to immature breccias that are mainly grain-supported. On the opposite, mature breccias have generally a convex grain size distribution and are matrix-supported (Henderson et al. 2010). The maturity is related to an increasing comminution of the particles and therefore to the longevity of a breccia. Henderson et al. (2010) have shown that the shear strength of the breccia decreases with increasing maturity.

Table 6: Summary of the grain size distribution analysis of the fine-grained breccia samples including the mean grain diameter and the diameter at the 10th, 50th and 90th percentiles (d10, d50 and d90, respectively), classification, distribution form and maturity of the breccia.

NGU sample #	Mean [µm]	d10 [µm]	d50 [µm]	d90 [µm]	Classification (Twiss and Moores, 2007)	Form of distribution	Textural maturity
47285	107.0	2.399	34.74	256.6	Microbreccia	Convex	Mature, matrix-supported
47286	134.3	3.622	32.43	251.4	Microbreccia	Convex	Mature, matrix-supported
47287	2328	4.279	82.50	11319	Breccia	Convex	Mature, matrix-supported
47288	4312	25.65	4005	11781	Breccia	Concave	Immature, grain-supported
47289	1013	19.00	224.1	3882	Breccia	Sigmoidal	Mature, matrix-supported
47290	6227	29.83	6511	14052	Breccia	Concave	Immature, grain-supported
47291	5409	17.25	4934	13562	Breccia	Concave	Immature, grain-supported
67353	7600	69.63	9034	14607	Breccia	Concave	Immature, grain-supported
67354	1695	3.847	48.63	10182	Breccia	Convex	Mature, matrix-supported
67355	1664	8.545	152.2	9496	Breccia	Convex	Mature, matrix-supported
67356	1177	3.402	33.31	4637	Breccia	Convex	Mature, matrix-supported
67357	1936	11.92	584.0	6234	Breccia	Linear	Mature, transitional
67358	149.3	1.692	21.30	168.8	Microbreccia	Convex	Mature, matrix-supported

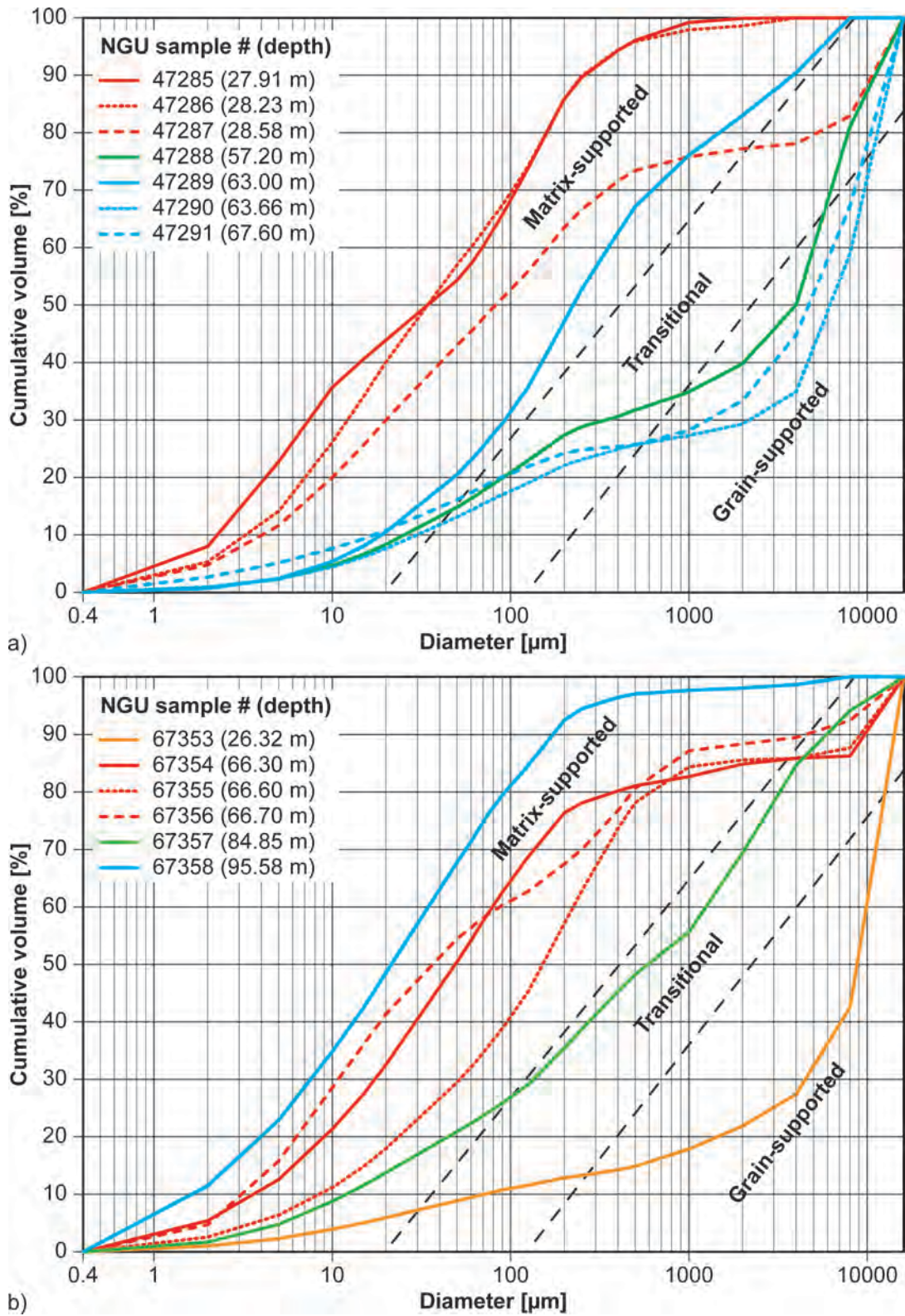


Figure 4: Grain size distributions from the breccia samples from a) borehole KH-01-10 and b) borehole KH-02-11. Samples from the same larger intervals with poor rock mass quality are plotted with the same colour. The limits between the matrix-supported, transitional and grain-supported domains from Henderson et al. (2010) are shown as dashed black lines.

The grain size distributions of the breccias samples from Mannen were analysed for their maturity (Table 6):

- All three samples from the 28–31 m depth interval (#47285, 47286 and 47287) with very poor rock mass quality in KH-01-10 are mature, matrix-supported microbreccias/breccias.
- The breccia at 57.20 m depth in KH-01-10 (#47288) is immature and grain-supported.
- The samples from the 62–64 m depth interval with very poor rock mass quality in KH-01-10 have different maturity. The upper sample at 63.00 m depth (#47289) is a mature, matrix-supported breccia, while the lower sample at 63.66 m depth (#47290) is an immature, grain-supported breccia.
- The breccia at 67.60 m depths in KH-01-10 (#47291) is immature and grain-supported.
- The breccia at 26.32 m depth in KH-02-11 (#67353) is immature and grain-supported.
- All three samples from the 66–67 m depth interval (#67354, 67355 and 67356) with poor rock mass quality in KH-02-11 are mature, matrix-supported breccias.
- The breccia at 84.85 m depth in KH-02-11 (#67357) falls into the transitional zone and has therefore medium maturity.
- The microbreccia at 95.58 m depth in KH-02-11 (#67358) is mature and matrix-supported.

The maturity of the breccia samples suggests that sliding occurred in the 27.90–28.61 m depth interval and at 63.00 m depth in KH-01-10, as well as in the 66.28–66.76 m depth interval and at 84.8 m and 95.58 m depth in KH-02-11. However, also the other heavily fractured, crushed and brecciated zones have undergone some deformation and sliding in the past. As stated by Saintot et al. (2011), the several cm-thick fine-grained breccia layers can not solely be explained by post-glacial creep movements, but also by chemical weathering of the gneisses. This alteration process is, however, favoured in severely fractured and crushed zones, which are generally observed above and below of the fine-grained breccia layers.

Figure 4 shows that there are more grain-supported, immature samples in the upper borehole KH-01-10 compared to the lower borehole KH-02-11 that has more matrix-supported, mature samples. The present knowledge on past and present slope deformations in depth does not allow to link these difference to different degrees of past deformation.

4.2.2 XRD analysis

The results from the XRD analysis of the breccia samples from Mannen are presented in Table 7. The raw data are given in the NGU-Lab analysis reports no. 2011.0039 and 2012.0060.

The main focus of the XRD analysis was the identification of clay minerals, such as smectite, illite, chlorite, kaolinite etc., but other major minerals, such as quartz, feldspars, amphibole etc., were also identified. A particular focus was given to smectite, because it is swelling clay mineral and will therefore have an effect on the stability of the rock slope depending on the water content. The identification of clay minerals in the breccia samples proved to be difficult due to relatively small clay quantities in some samples and overlapping reflections from different clay minerals. This overlapping of reflections may be due to the fact that the clay minerals have not yet stabilized, but are still in the change from one mineral to the other. Since the material has been mechanically altered by creep and/or sliding such diversity in stages of the clay minerals is possible.

Following clay minerals were identified in the upper borehole (KH-01-10):

- Chlorite and talc are identified in the samples #47285 and 47290. Talc can be formed by a metamorphic reaction involving chlorite and quartz under high temperature and pressure.
- Chlorite, illite and illite-montmorillonite are the clay minerals in samples #47286 and 47287. Montmorillonite is part of the smectite group (swelling clays) and occur often intermixed with illite, making a clear distinction difficult.
- Chlorite is the only clay mineral present in sample #47288.
- The sample #47289 contained too little material in the clay fraction for a XRD analysis.

Following clay minerals were identified in the lower borehole (KH-02-11):

- Chlorite and illite are the main clay minerals in the samples #67354, 67355 and 67358. Chlorite can be clearly distinguished from kaolinite in the glycolated and heated samples.
- Smectite and chlorite are found in sample #67356 (taken at 66.70 m depth). Smectite is a swelling clay mineral and shows a typical behaviour with an increase in lattice spacing from 14.1 Å to 16.0 Å in the glycolated sample, followed by a reduction to 9.9 Å in the heated sample.
- Illite is the only clay mineral in sample #67357, even though there are slight hints for the presence of chlorite.
- The sample #67353 contained too little material in the clay fraction for a XRD analysis.

The presence of chlorite in most fine-grained breccia samples is not surprising since the encountered lithologies often contain chlorite from retrograde metamorphism (see section 2.1.1, Table 2 and Appendix 2). In contrast, illite and smectite are typical weathering products of mica and feldspar and are thus relatively newly formed. It is interesting to see that the samples with clear clay mineral content in the form of illite or smectite (including illite-montmorillonite) are mature, matrix-supported breccias based on the grain size distribution (see section 4.2.1, Figure 4).

Table 7: Summary of the XRD analysis of the fine-grained breccia samples with the identified possible main minerals, likely minerals and other possible minerals. Minerals of the clay group are underlined.

NGU sample #	Possible main minerals	Likely minerals	Other possible minerals
47285	Amphibole, calcite		Mica, <u>chlorite</u> , <u>talc</u>
47286	Amphibole, <u>chlorite</u>	Calcite	<u>Illite</u> , <u>illite-montmorillonite</u> , feldspar
47287	Amphibole, <u>chlorite</u>	Calcite, quartz, <u>illite</u>	<u>Illite-montmorillonite</u> , feldspar
47288	Feldspar, calcite, quartz, <u>chlorite</u>	Biotite	
47289	<i>Too little material for XRD analysis</i>		
47290	Calcite, amphibole, <u>chlorite</u>	Quartz	<u>Talc</u> , mica, feldspar
47291	Quartz, feldspar, calcite, mica	<u>Chlorite</u>	Amphibole
67353	<i>Too little material for XRD analysis</i>		
67354	Quartz, <u>chlorite</u> , calcite	<u>Illite</u>	Amphibole, feldspar
67355	<u>Chlorite</u> , quartz	Calcite, <u>illite</u>	Amphibole
67356	<u>Smectite</u> , calcite, <u>chlorite</u>		Quartz
67357	Calcite, quartz, <u>illite</u>		
67358	Calcite, quartz, <u>chlorite</u> , <u>illite</u>	Plagioclase	Hornblende

5. CONCLUSIONS & RECOMMENDATIONS

The geological and engineering geological logging of the drill core of the lower borehole (KH-02-11) at Mannen unstable rock slope shows several zones of damaged rocks. Large intervals with crushed rocks containing fine-grained breccias were observed at 26 m, 66 m, 84 m and 95 m depth in KH-02-11. The core logging of KH-02-11 revealed significant differences with the upper borehole at Mannen (KH-01-10) in terms of degree of folding, orientation of foliation and sequence of lithologies.

The grain size distribution analyses and XRD analyses of fine-grained breccias encountered in the drill cores of both boreholes at Mannen indicate several zones with mature, matrix-supported breccias or microbreccias that contain illite and sometimes also smectite as clay minerals. These zones are likely the locations of past displacements of the unstable rock slope at 27.90–28.61 m and 63.00 m depth in the upper borehole (KH-01-10) and at 66.28–66.76 m, 84.80 m and 95.58 m depth in the lower borehole (KH-02-11). Illite is the common clay mineral in several of the fine-grained breccia samples. Swelling clay minerals of the smectite group are encountered at 28.23 m and 28.58 m depth in KH-01-10 and 66.70 m depth in KH-02-11. A basal sliding surface might be located at 28 m depth in KH-01-10 based on borehole displacement measurements (Kristensen and Blikra 2011), as well as at 66 m depth in KH-02-11 based on the geological and engineering geological core logging presented in this report.

The geological model of the Mannen unstable rock slope and the different considered scenarios needs to be updated by integrating the results from the geological and engineering geological core logging and the optical televiewer borehole logging of both boreholes. This geological model needs also to incorporate various displacement measurements (GPS measurements, laser distancemeters, extensometers, ground-based InSAR etc.), structural field mapping, geomorphologic analysis, electric resistivity data and other available data.

6. REFERENCES

- Dahle, H., Anda, E., Saintot, A. and Sætre, S. (2008) Faren for fjellskred fra fjellet Mannen i Romsdalen. NGU report 2008.087, Geological Survey of Norway, Trondheim, Norway.
- Dahle, H., Bjerke, P.L., Crosta, G.B., Hermanns, R.L., Anda, E. and Saintot, A. (2011a) Faresoner for utløp, oppdemming og flom som følge av fjellskredfare ved Mannen. NGU report 2011.058, Geological Survey of Norway, Trondheim, Norway.
- Dahle, H., Saintot, A., Blikra, L.H. and Anda, E. (2011b) Geofagleg oppfølging av ustabil fjellparti ved Mannen i Romsdalen. NGU report 2010.022, Geological Survey of Norway, Trondheim, Norway.
- Dalsegg, E. and Rønning, J.S. (2012) Geofysiske målinger på Mannen i Rauma kommune, Møre og Romsdal. NGU report 2012.024, Geological Survey of Norway, Trondheim, Norway.
- Deere, D.U. (1964) Technical description of rock cores for engineering purposes. *Rock Mechanics and Engineering Geology*, **1**, 1, 16-22.
- Elvebakk, H. (2012) Borhullslogging med optisk viewer KH-02-11, Mannen, Rauma kommune, Møre og Romsdal. NGU report 2012.032, Geological Survey of Norway, Trondheim, Norway.
- Farsund, T.Ø. (2011) Geological and numerical stability modelling of Mannen, Romsdalen. MSc, Norwegian University of Science and Technology, Trondheim, Norway.
- Henderson, I. and Saintot, A. (2007) Fjellskredundersøkelser i Møre og Romsdal. NGU report 2007.043, Geological Survey of Norway, Trondheim, Norway.
- Henderson, I.H.C., Ganerød, G.V. and Braathen, A. (2010) The relationship between particle characteristics and frictional strength in basal fault breccias: Implications for fault-rock evolution and rockslide susceptibility. *Tectonophysics*, **486**, 1-4, 132-149.
- Jaeger, J.C. and Cook, N.G.W. (1963) Pinching-off and diking of rocks. *Journal of Geophysical Research*, **68**, 6, 1759-1765.
- Kristensen, L. and Blikra, L.H. (2011) Monitoring displacement on the Mannen rockslide in Western Norway. In: Catani, F., Marggottini, C., Trigila, A. and Iadanza, C. (eds.) *Proceedings of the Second World Landslide Forum*, ISPRA - Italian National Institute for Environmental Protection and Research, Rome, Italy, pp. WLF2-2011-0381.
- Saintot, A., Elvebakk, H., Oppikofer, T., Ganerød, G.V. and Farsund, T.Ø. (2011) Mannen unstable rock slope (Møre & Romsdal): Logging of borehole and drill core KH-01-10, geomorphologic digital elevation model interpretation & displacement analysis by terrestrial laser scanning. NGU report 2011.026, Geological Survey of Norway, Trondheim, Norway.
- Twiss, R.J. and Moores, E.M. (2007) *Structural Geology*, 2nd edition, W. H. Freeman and Company, New York, 736 pp.

APPENDIXES

Appendix 1: Pictures of the drill core of borehole KH-02-11 with observations of the geological and engineering geological core logging

The figures in Appendix 1 show the photographs of the drill cores of borehole KH-02-11 at Mannen. The dry cores are on the left side, while the wet cores are on the right side. Geological and engineering geological observations annotated next to the drill core photographs include lithological descriptions (black text), structural observations such as folds or changes in foliation dip angle (green text), as well as severely fractured or crushed zones, fine-grained breccia zones and core loss (red text).

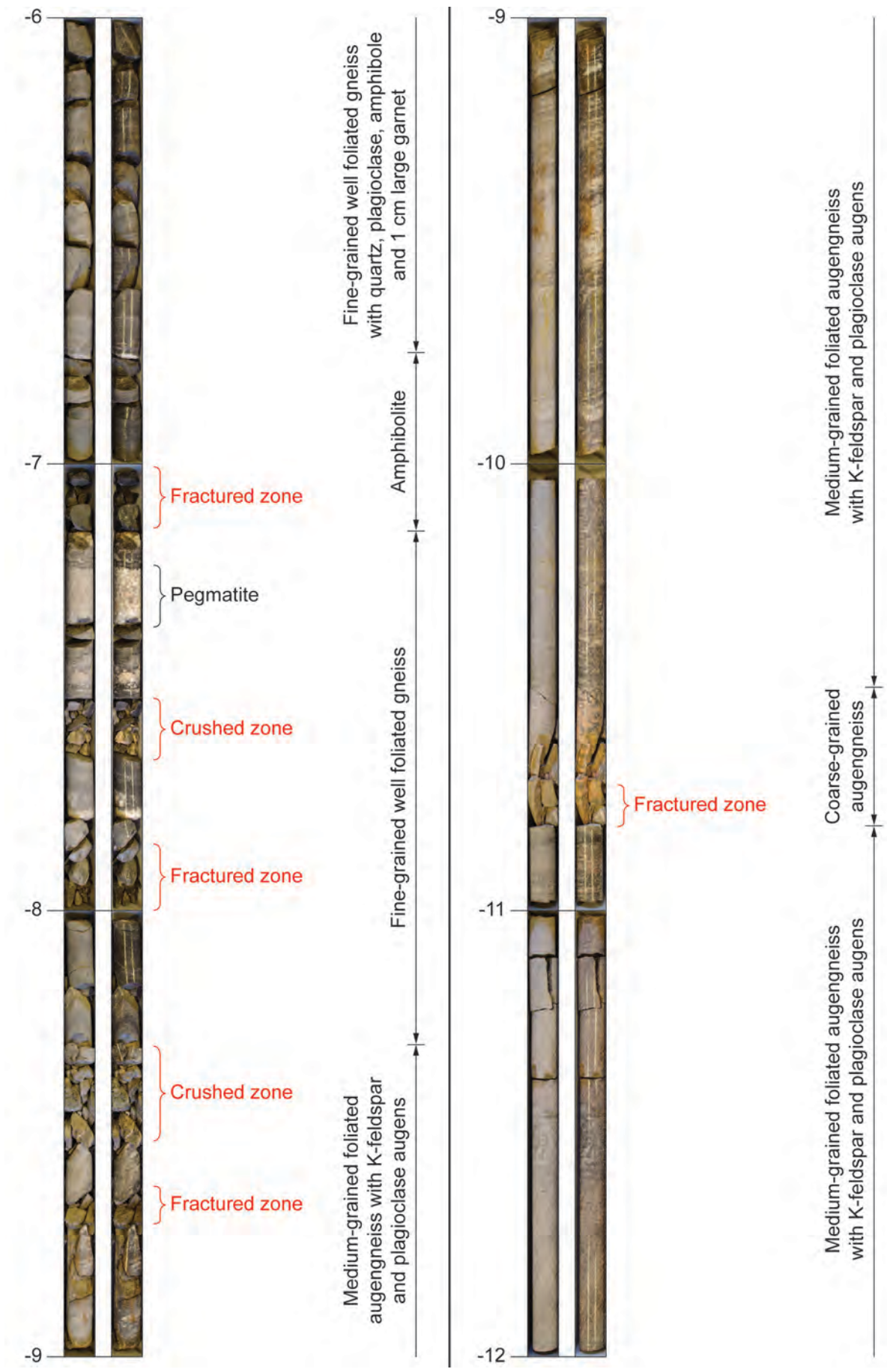


Figure A1.1: Geological and engineering geological core logging from 6 to 12 m depth with pictures of the dry (left) and wet (right) core.

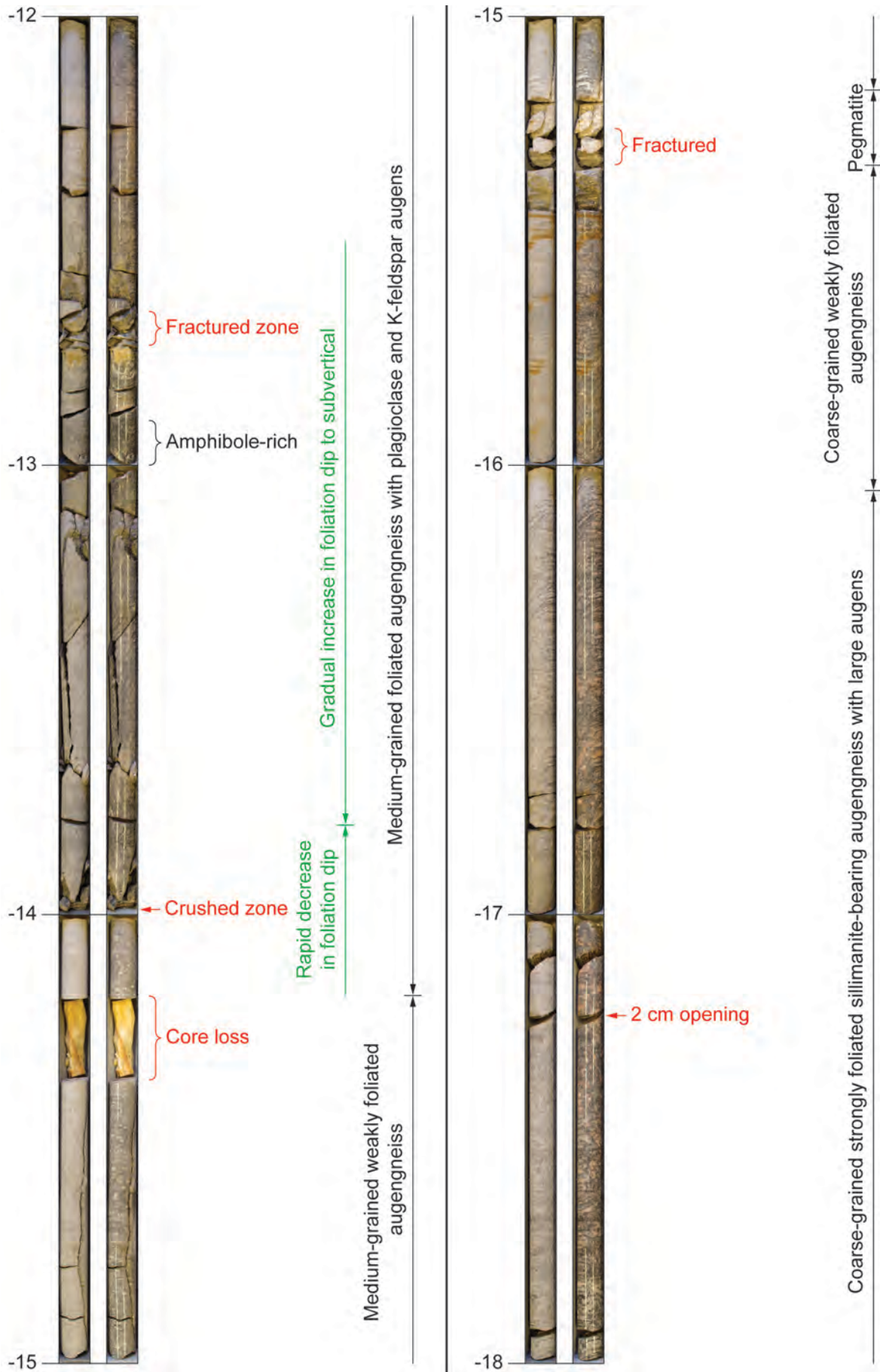


Figure A1.2: Geological and engineering geological core logging from 12 to 18 m depth with pictures of the dry (left) and wet (right) core.

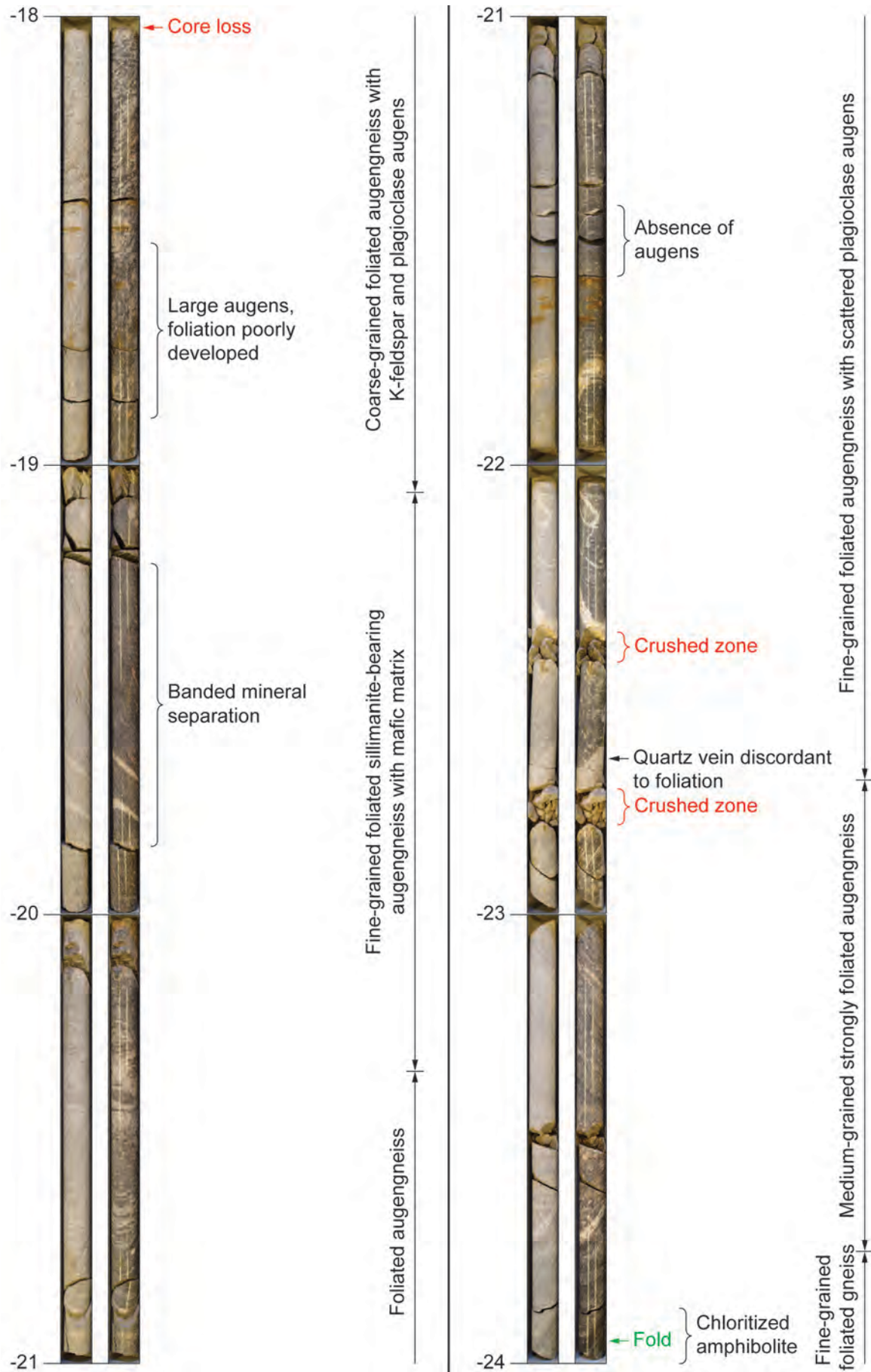


Figure A1.3: Geological and engineering geological core logging from 18 to 24 m depth with pictures of the dry (left) and wet (right) core.

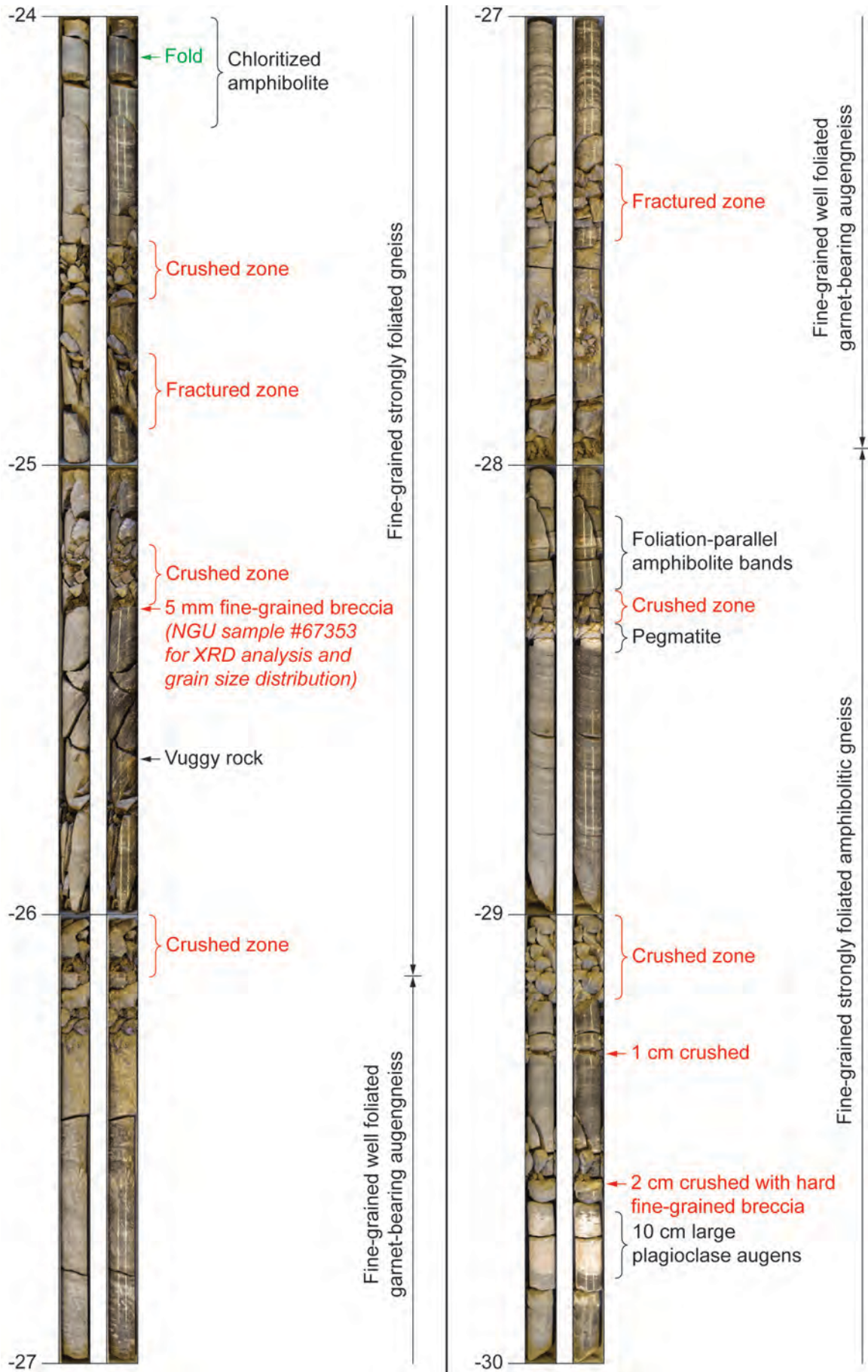


Figure A1.4: Geological and engineering geological core logging from 24 to 30 m depth with pictures of the dry (left) and wet (right) core.

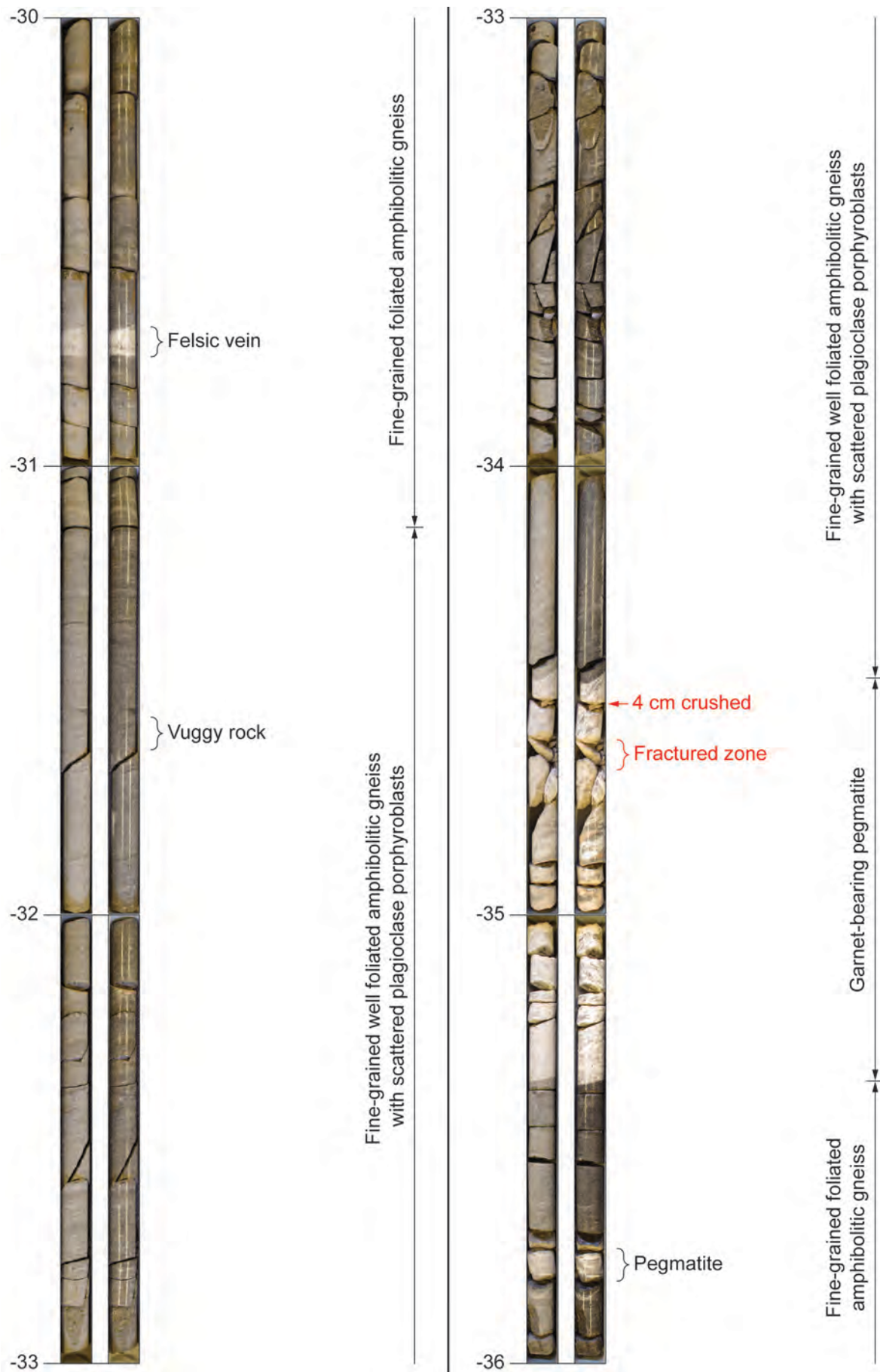


Figure A1.5: Geological and engineering geological core logging from 30 to 36 m depth with pictures of the dry (left) and wet (right) core.

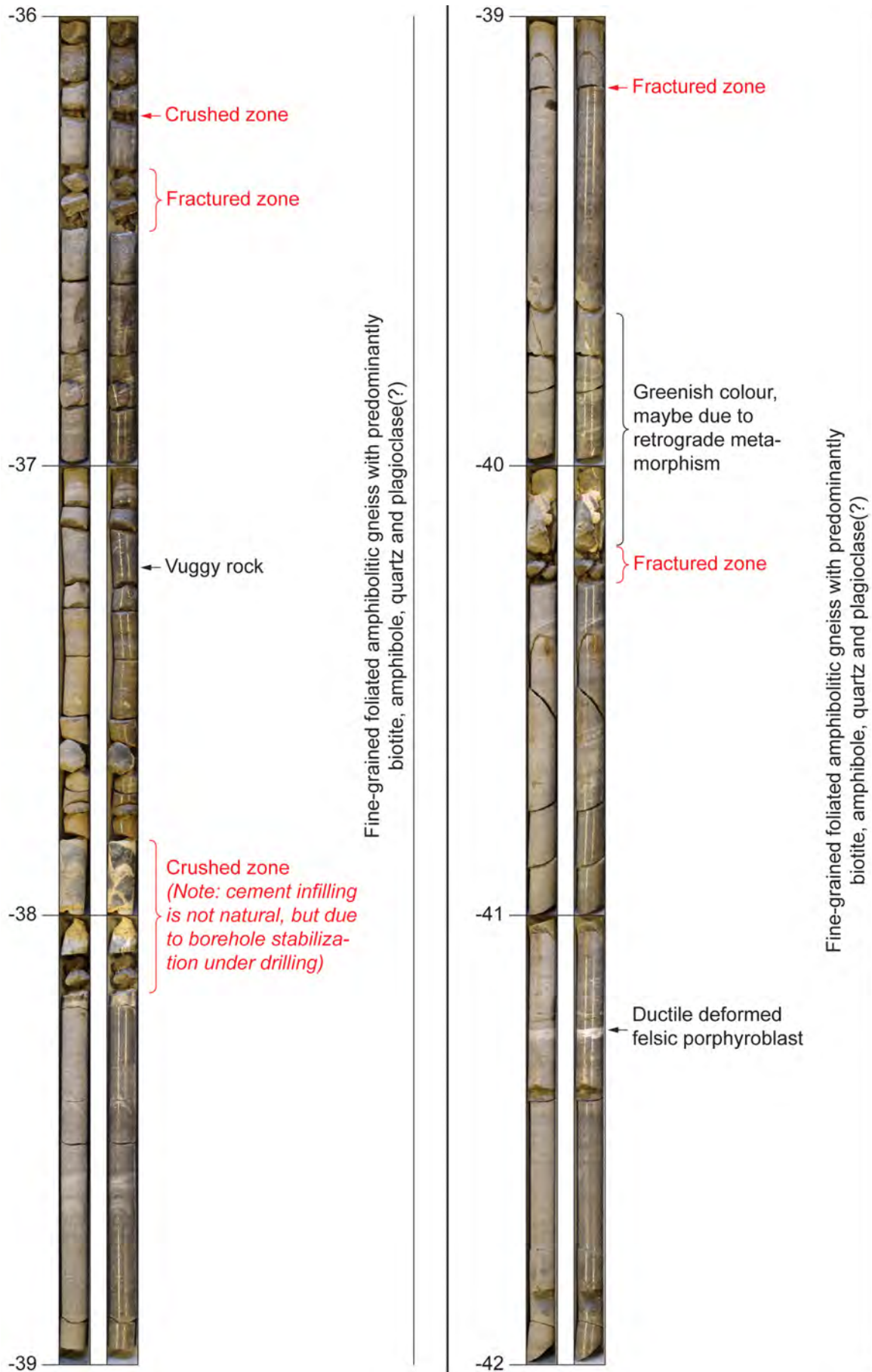


Figure A1.6: Geological and engineering geological core logging from 36 to 42 m depth with pictures of the dry (left) and wet (right) core.

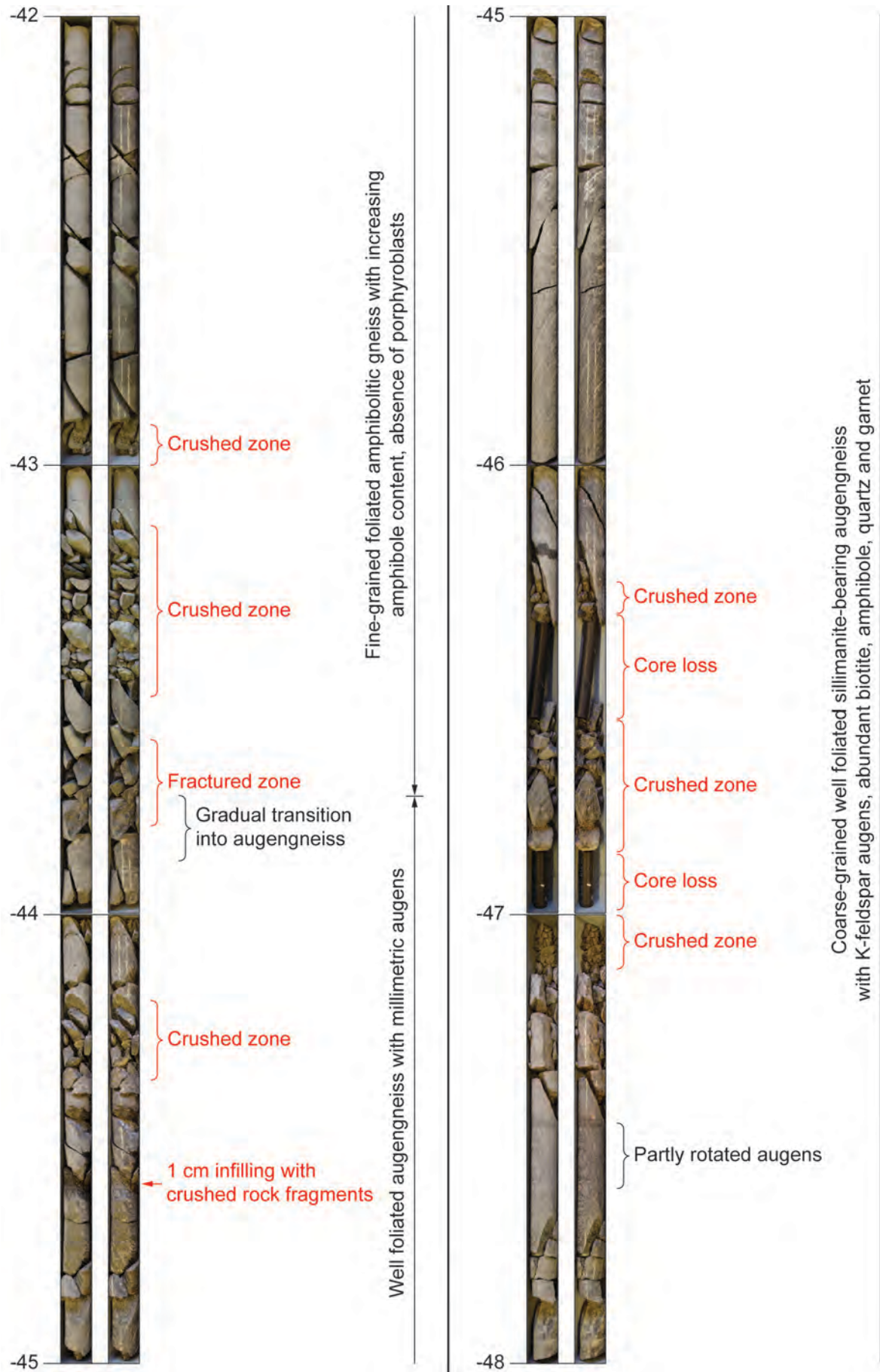


Figure A1.7: Geological and engineering geological core logging from 42 to 48 m depth with pictures of the dry (left) and wet (right) core.

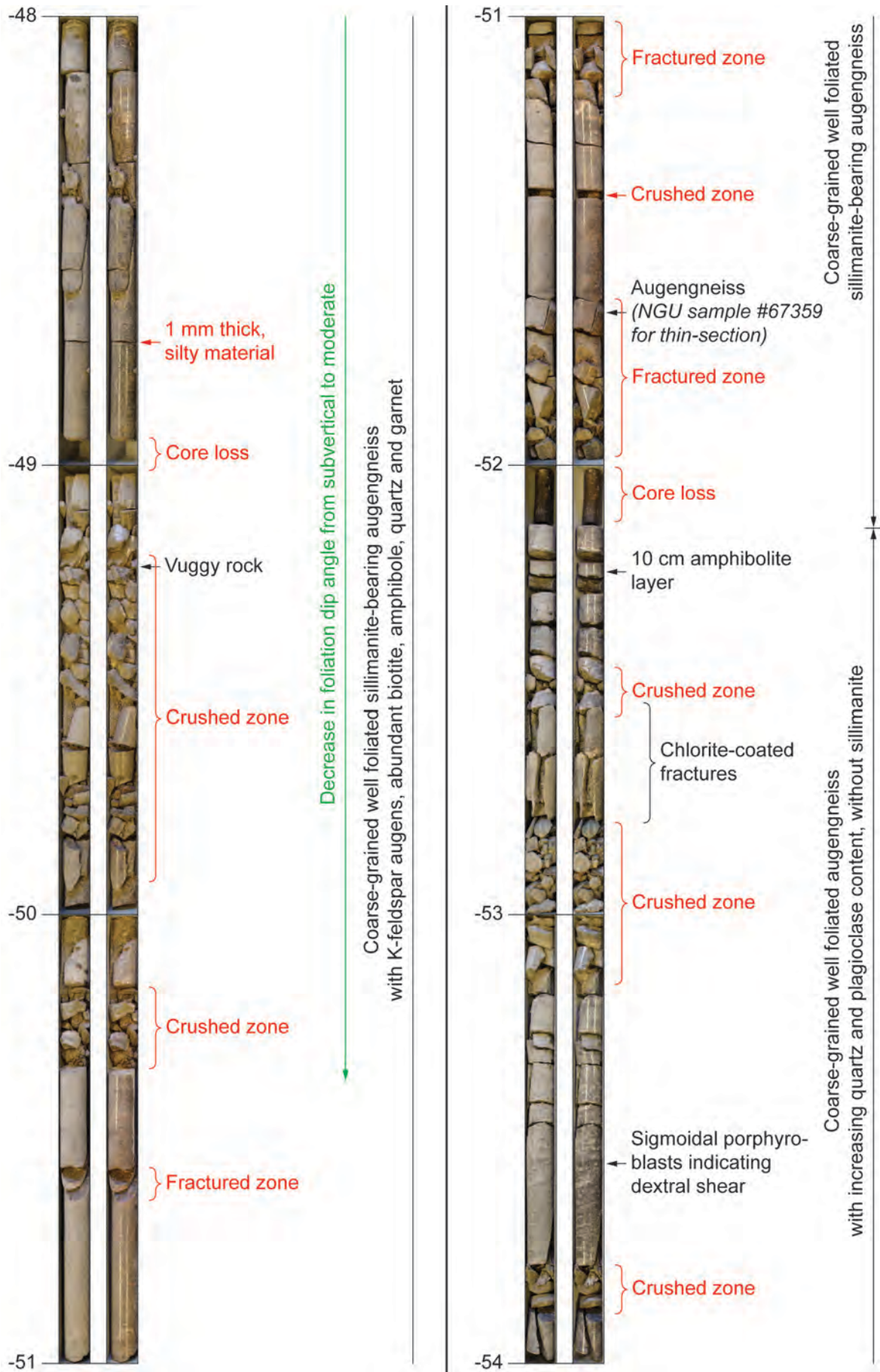


Figure A1.8: Geological and engineering geological core logging from 48 to 54 m depth with pictures of the dry (left) and wet (right) core.

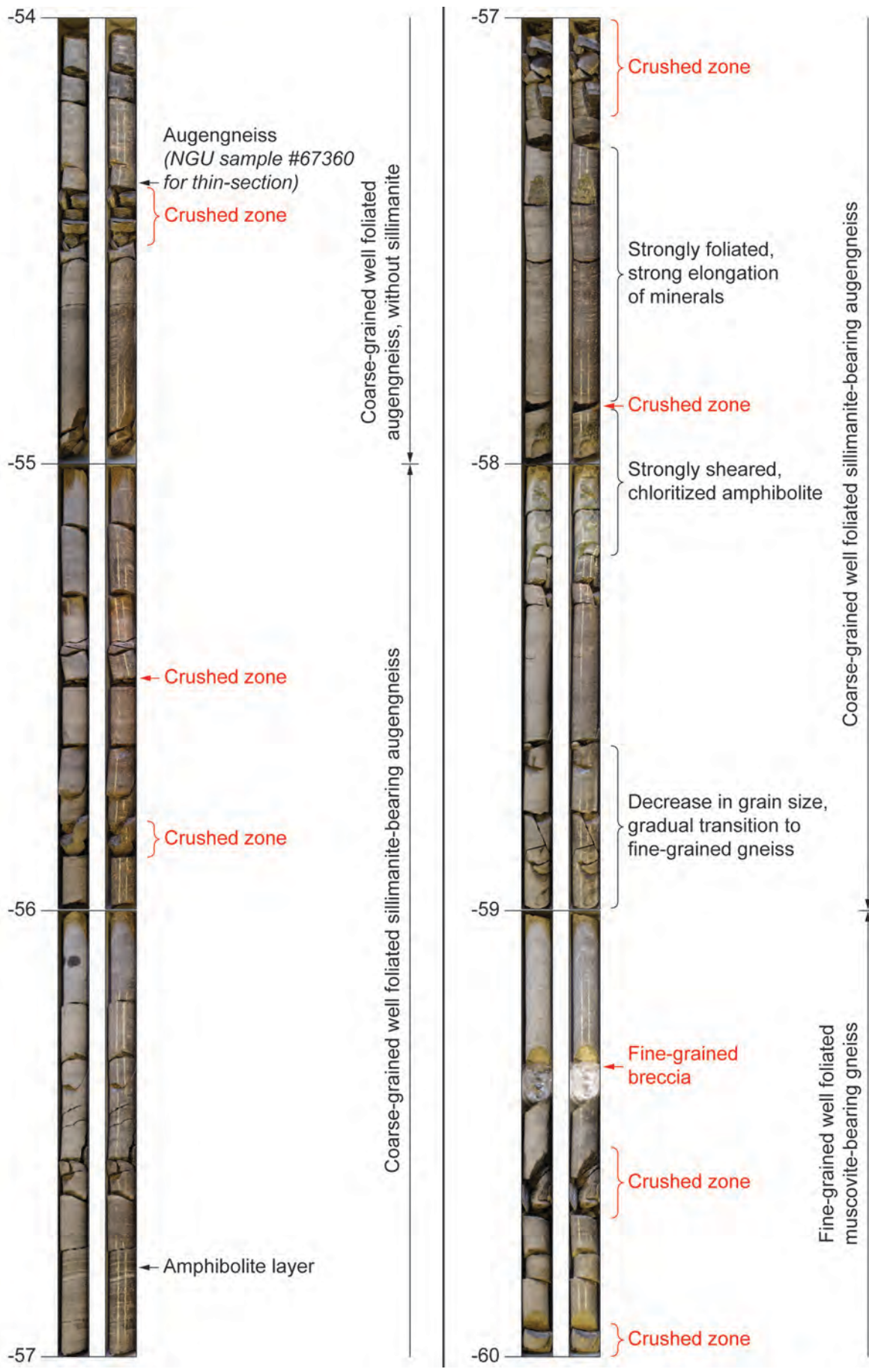


Figure A1.9: Geological and engineering geological core logging from 54 to 60 m depth with pictures of the dry (left) and wet (right) core.

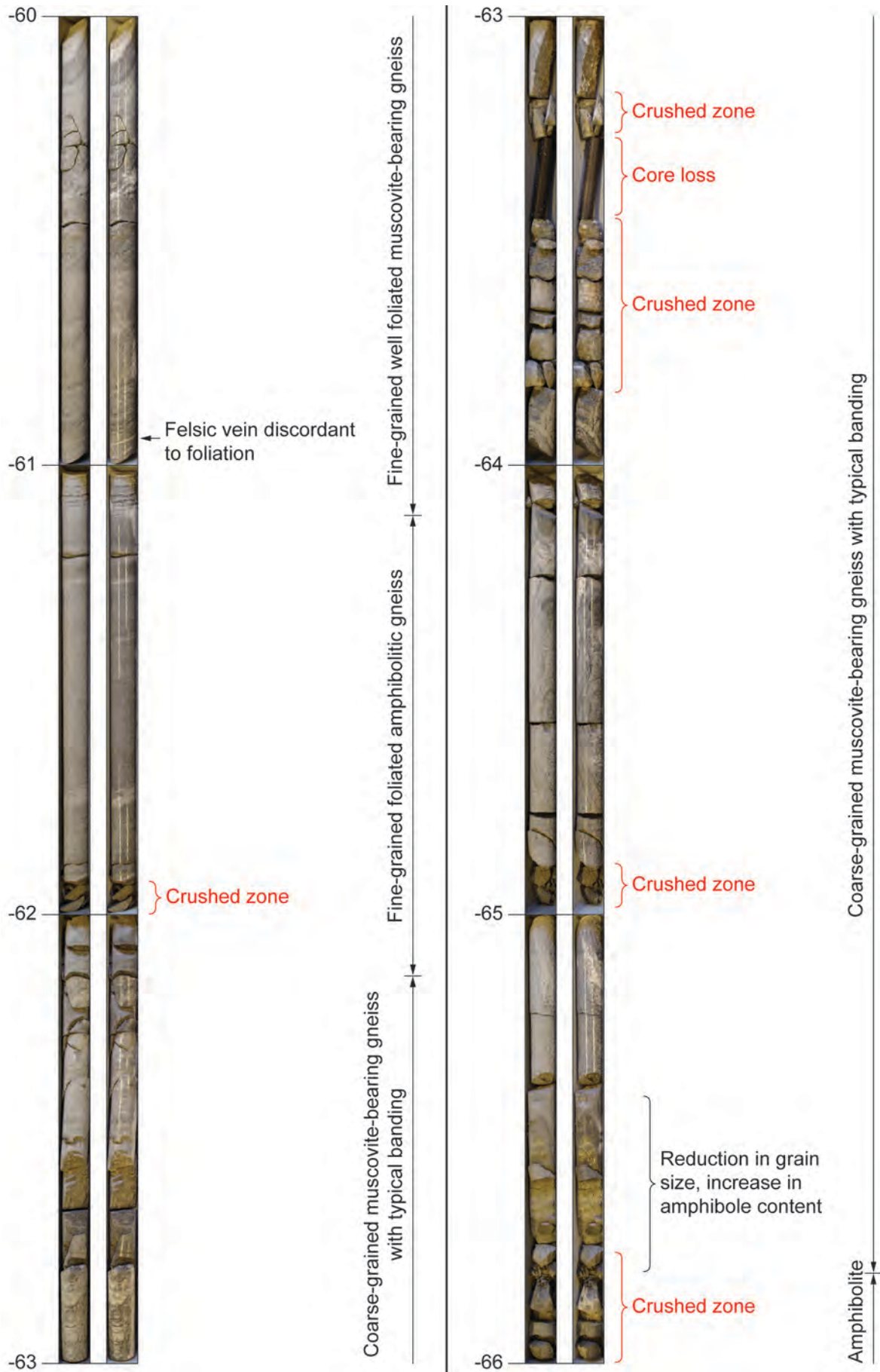


Figure A1.10: Geological and engineering geological core logging from 60 to 66 m depth with pictures of the dry (left) and wet (right) core.

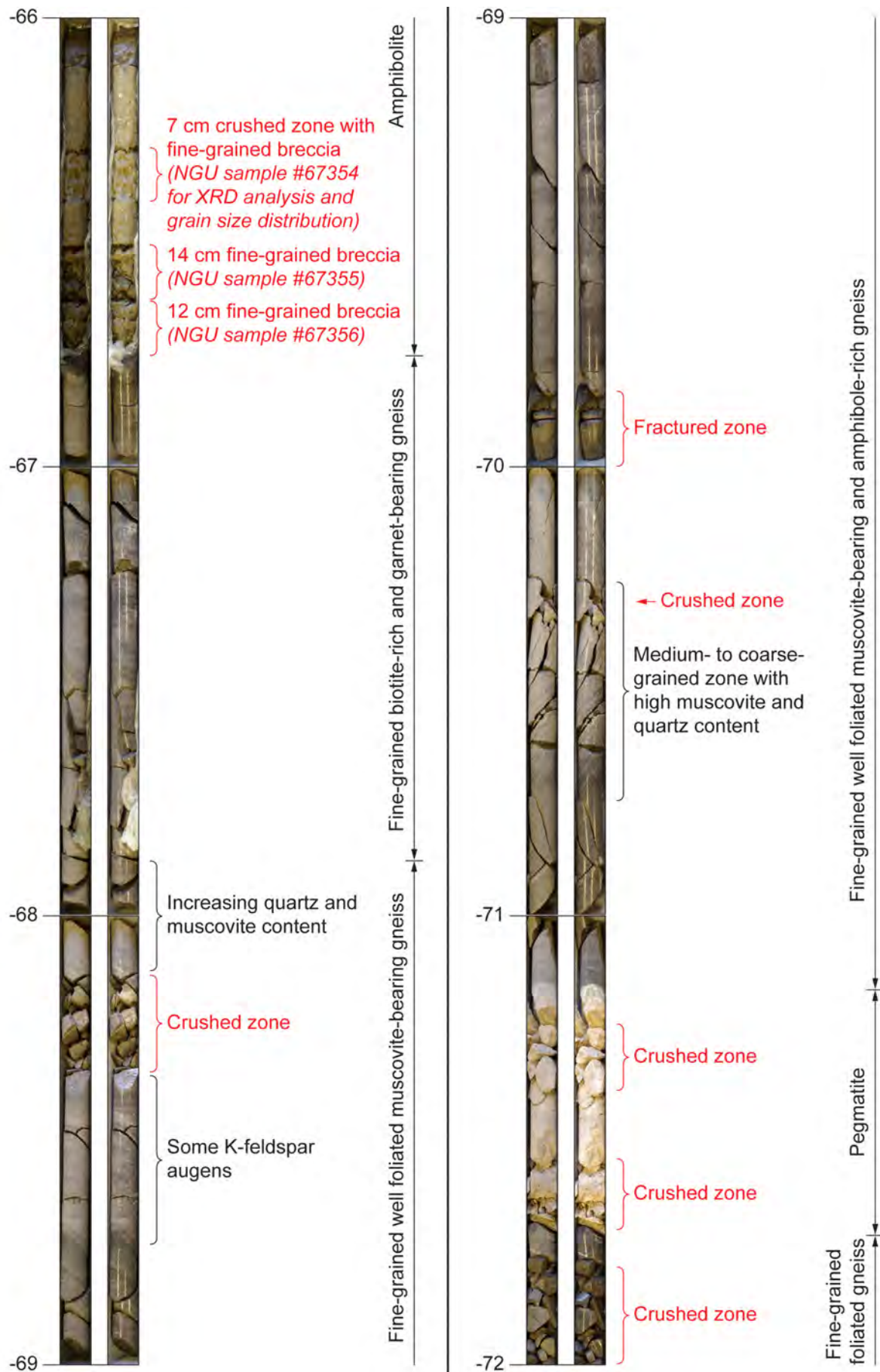


Figure A1.11: Geological and engineering geological core logging from 66 to 72 m depth with pictures of the dry (left) and wet (right) core.

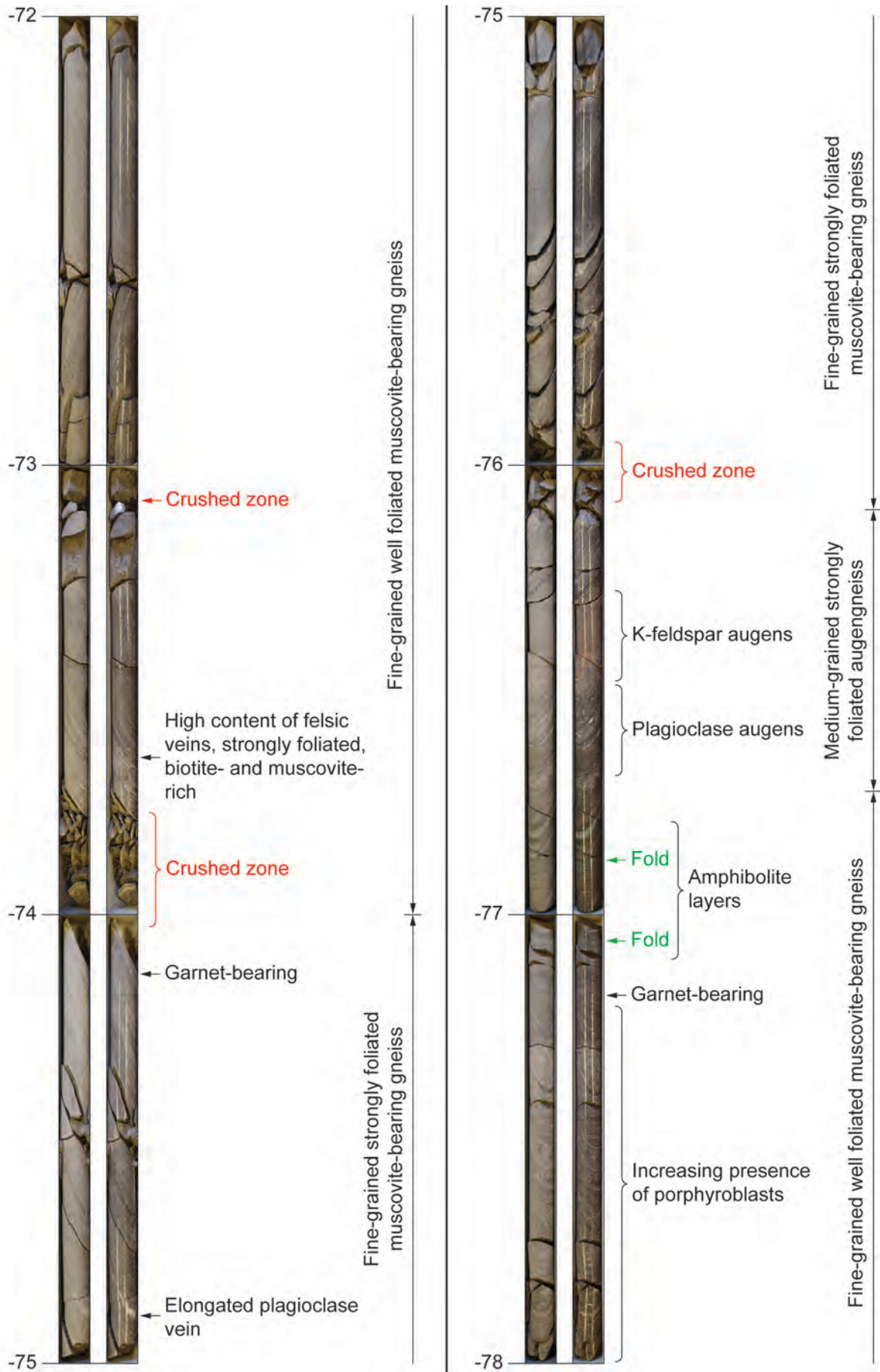


Figure A1.12: Geological and engineering geological core logging from 72 to 78 m depth with pictures of the dry (left) and wet (right) core.

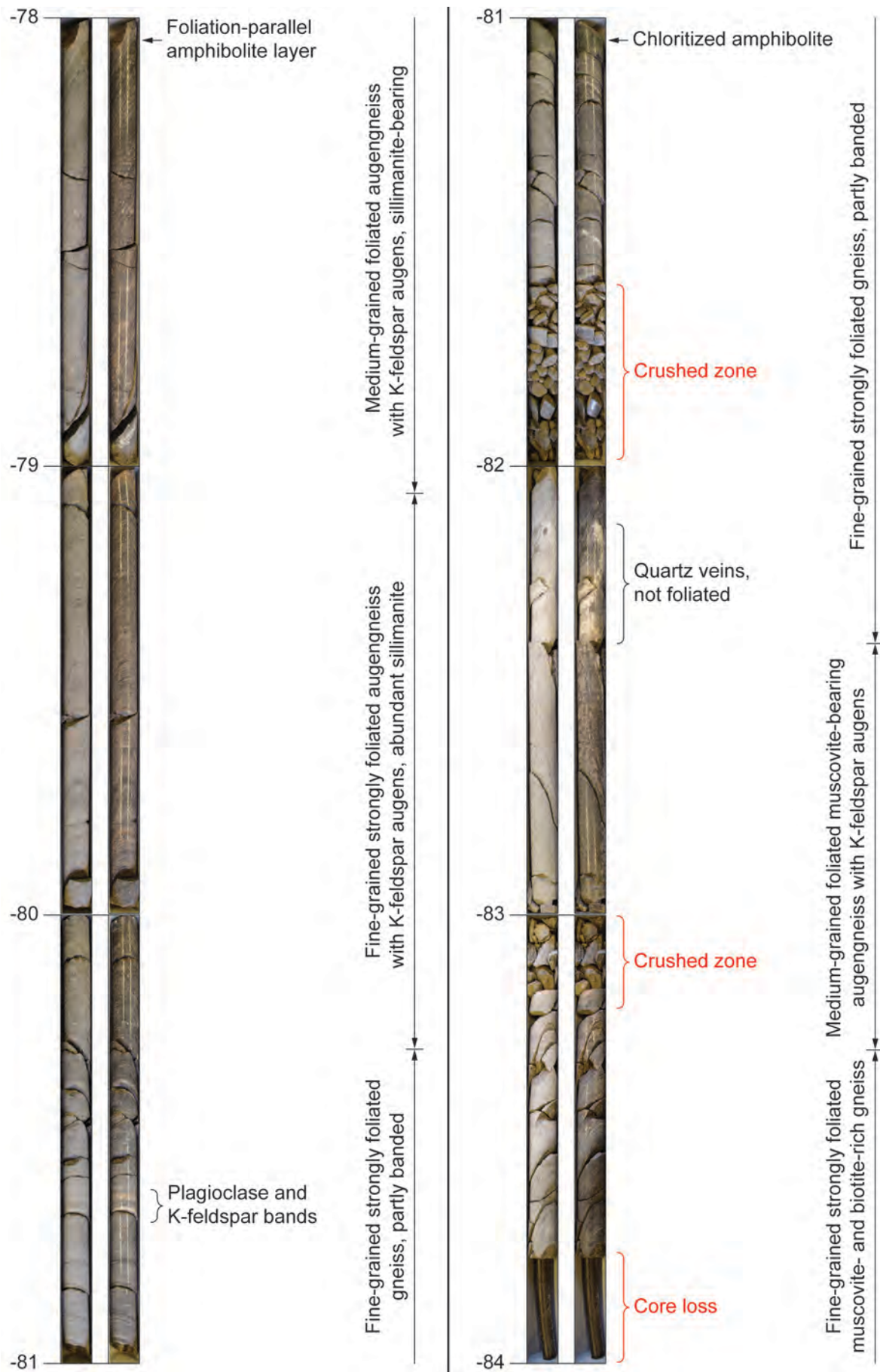


Figure A1.13: Geological and engineering geological core logging from 78 to 84 m depth with pictures of the dry (left) and wet (right) core.

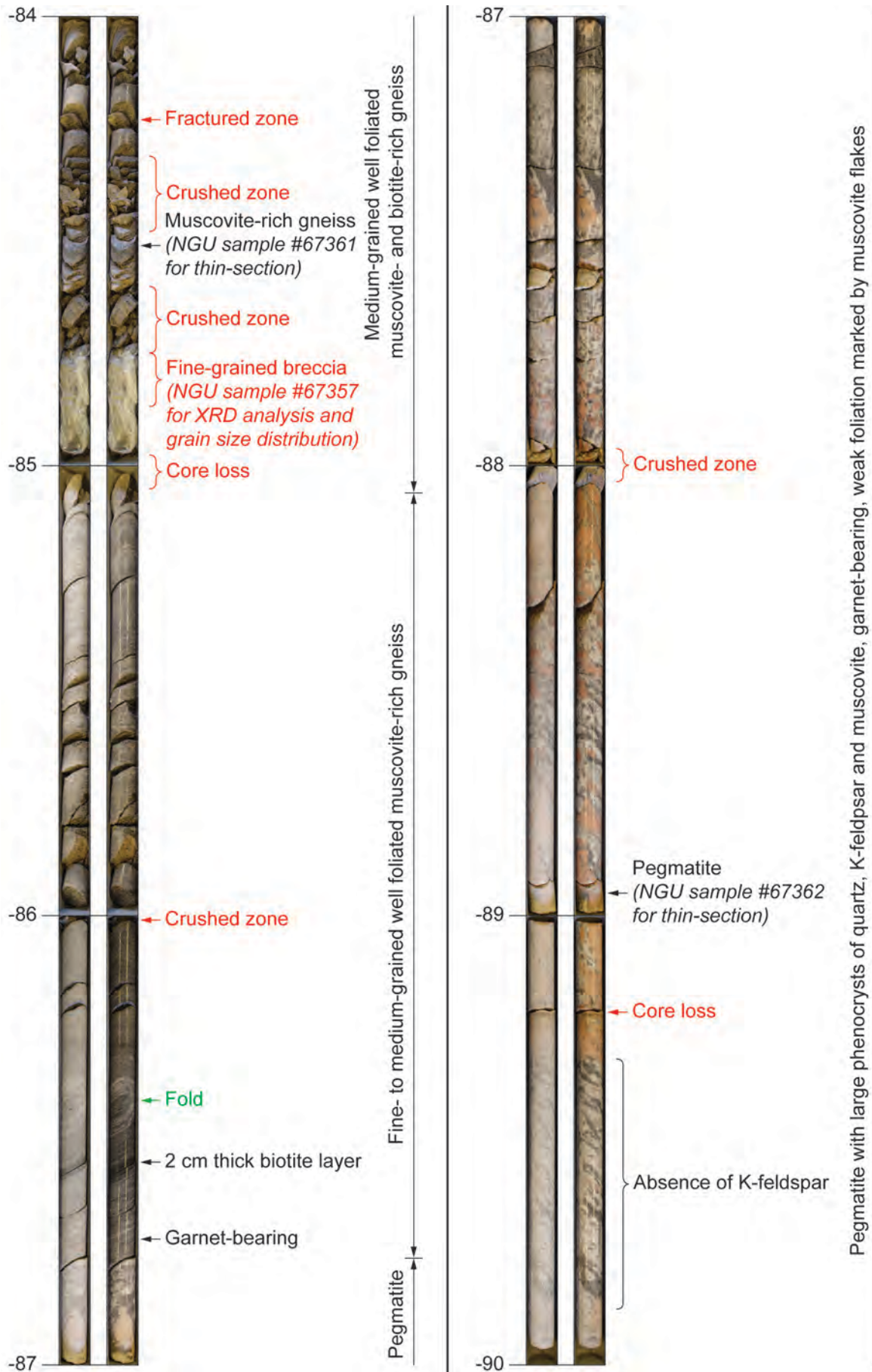


Figure A1.14: Geological and engineering geological core logging from 84 to 90 m depth with pictures of the dry (left) and wet (right) core.

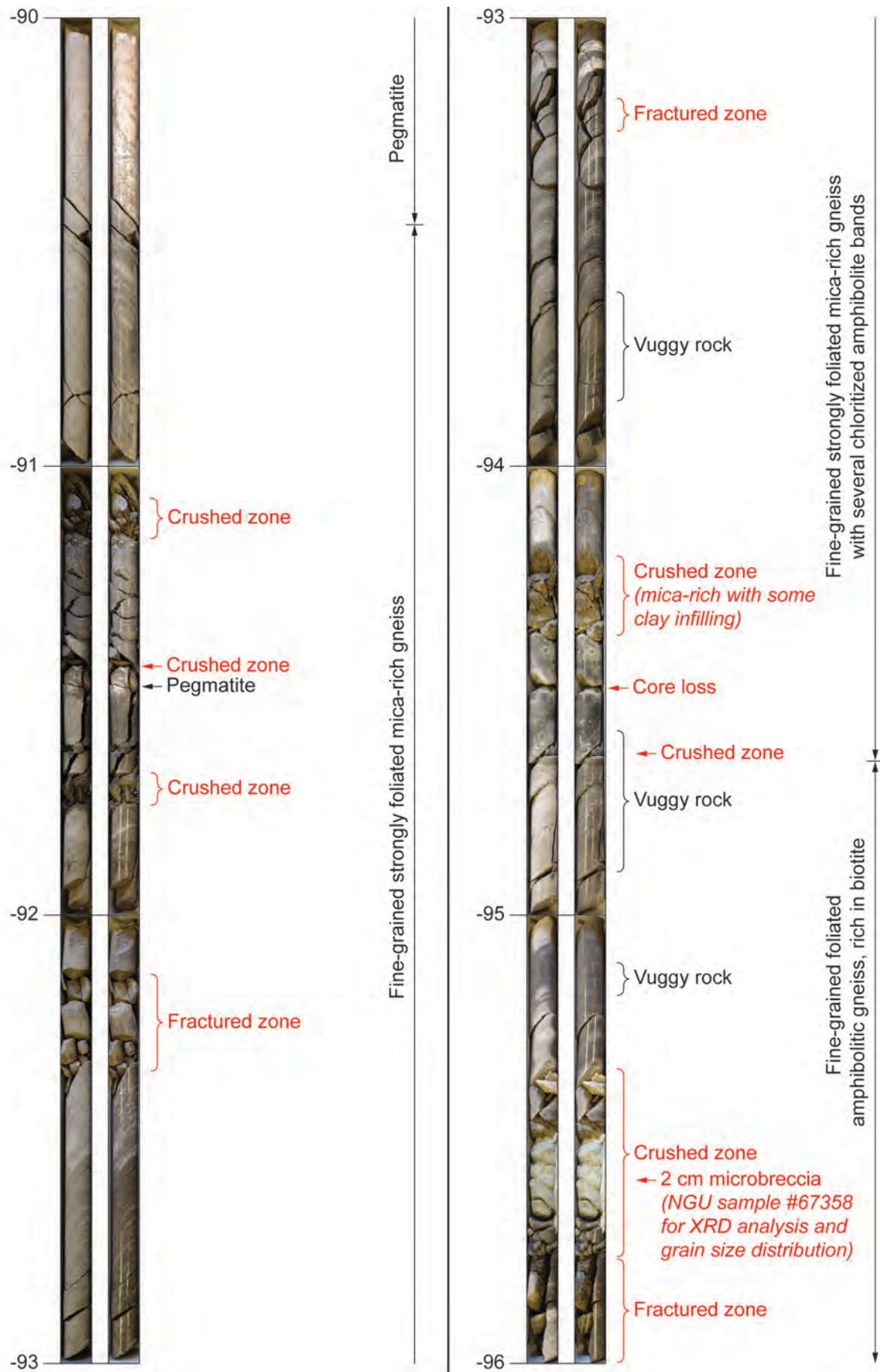


Figure A1.15: Geological and engineering geological core logging from 90 to 96 m depth with pictures of the dry (left) and wet (right) core.

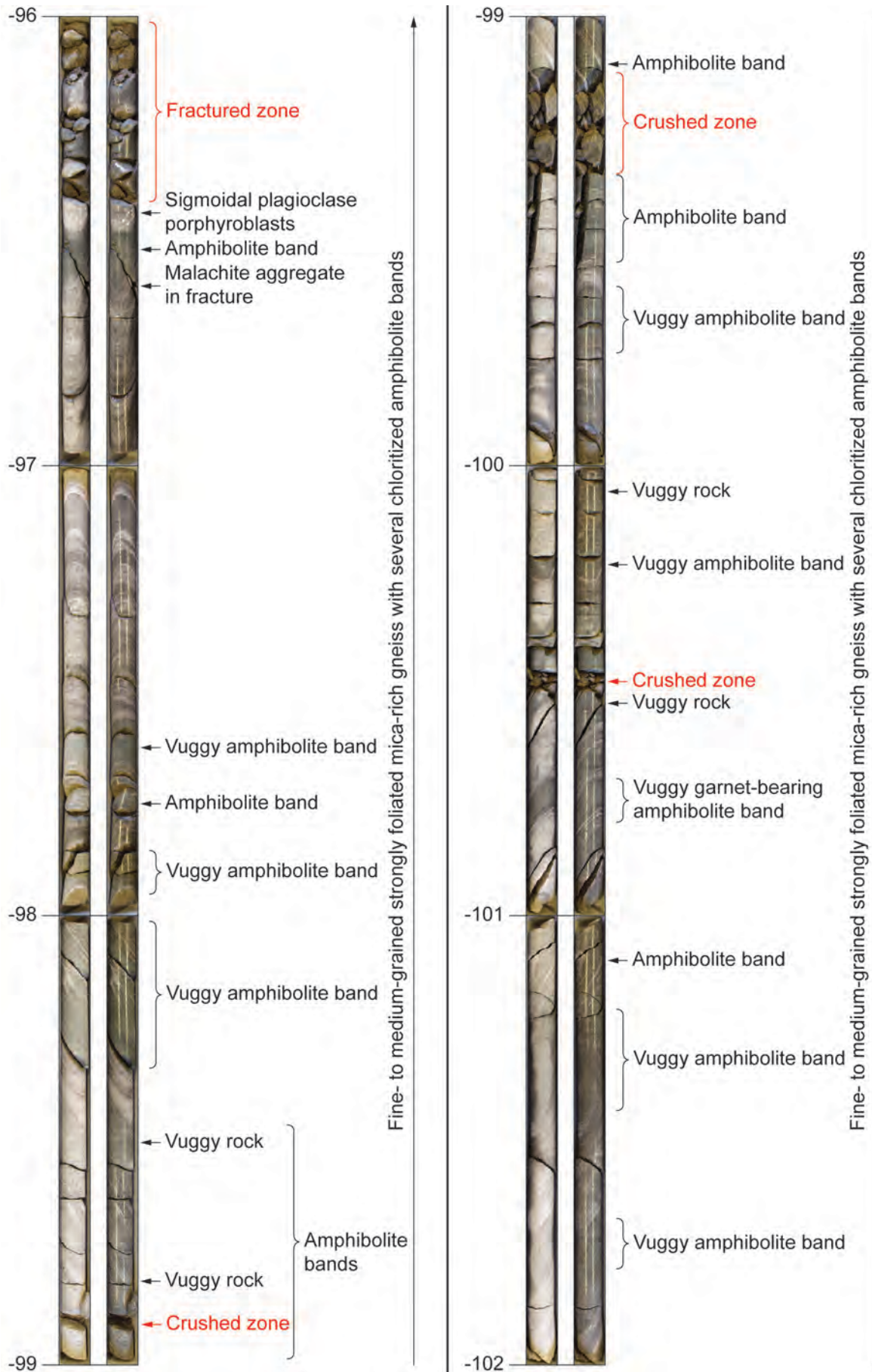


Figure A1.16: Geological and engineering geological core logging from 96 to 102 m depth with pictures of the dry (left) and wet (right) core.

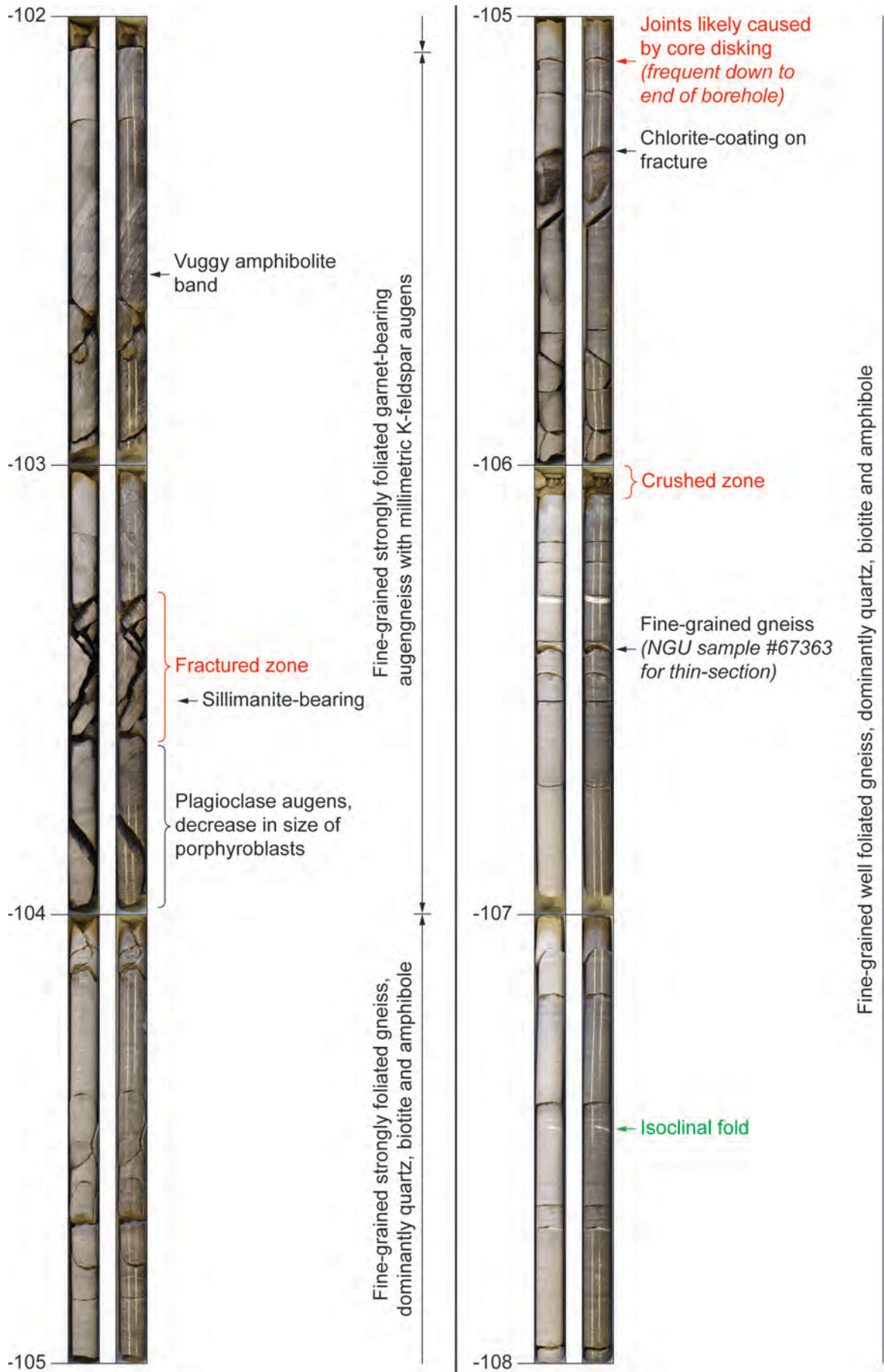


Figure A1.17: Geological and engineering geological core logging from 102 to 108 m depth with pictures of the dry (left) and wet (right) core.

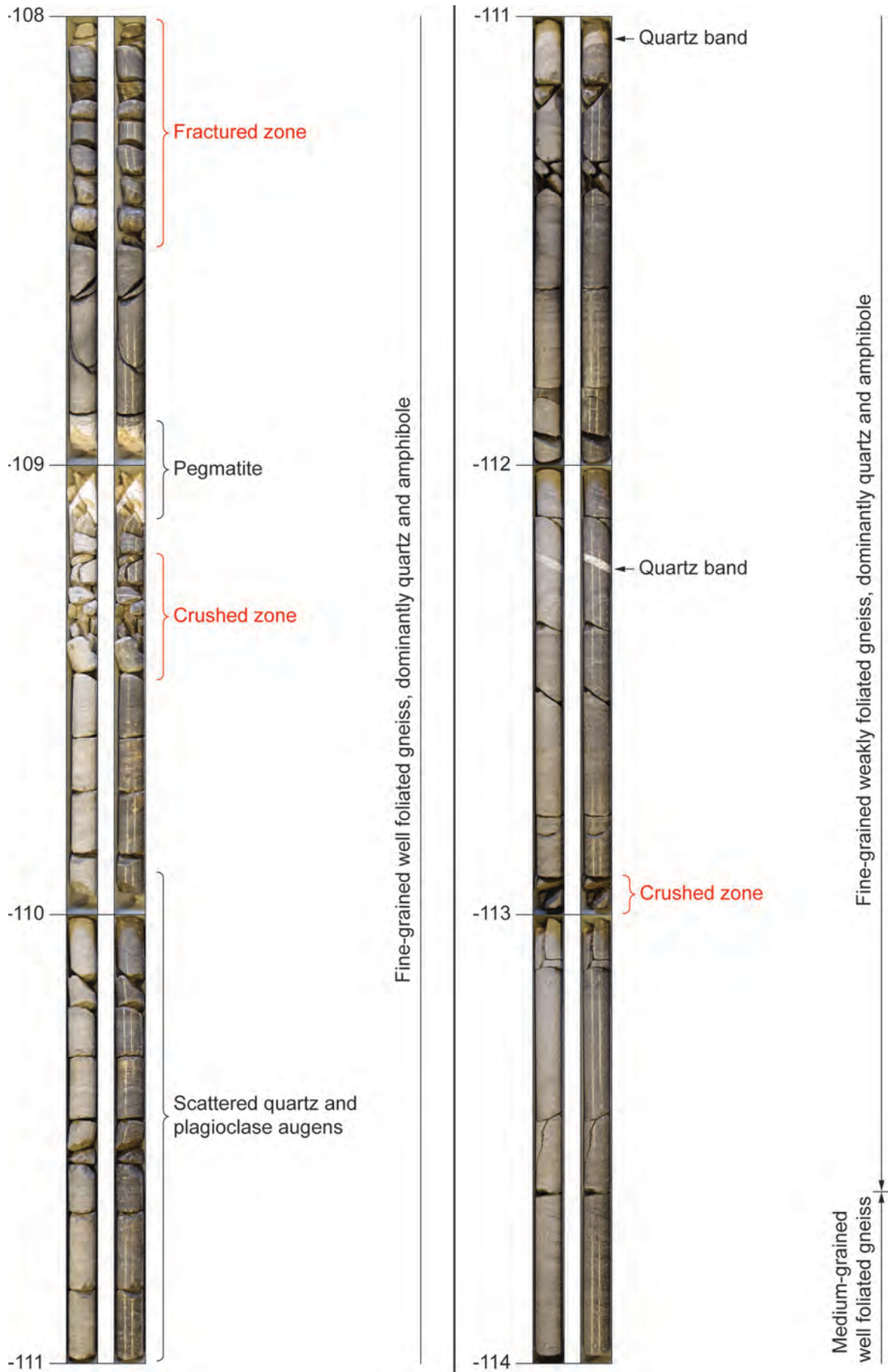


Figure A1.18: Geological and engineering geological core logging from 108 to 114 m depth with pictures of the dry (left) and wet (right) core.

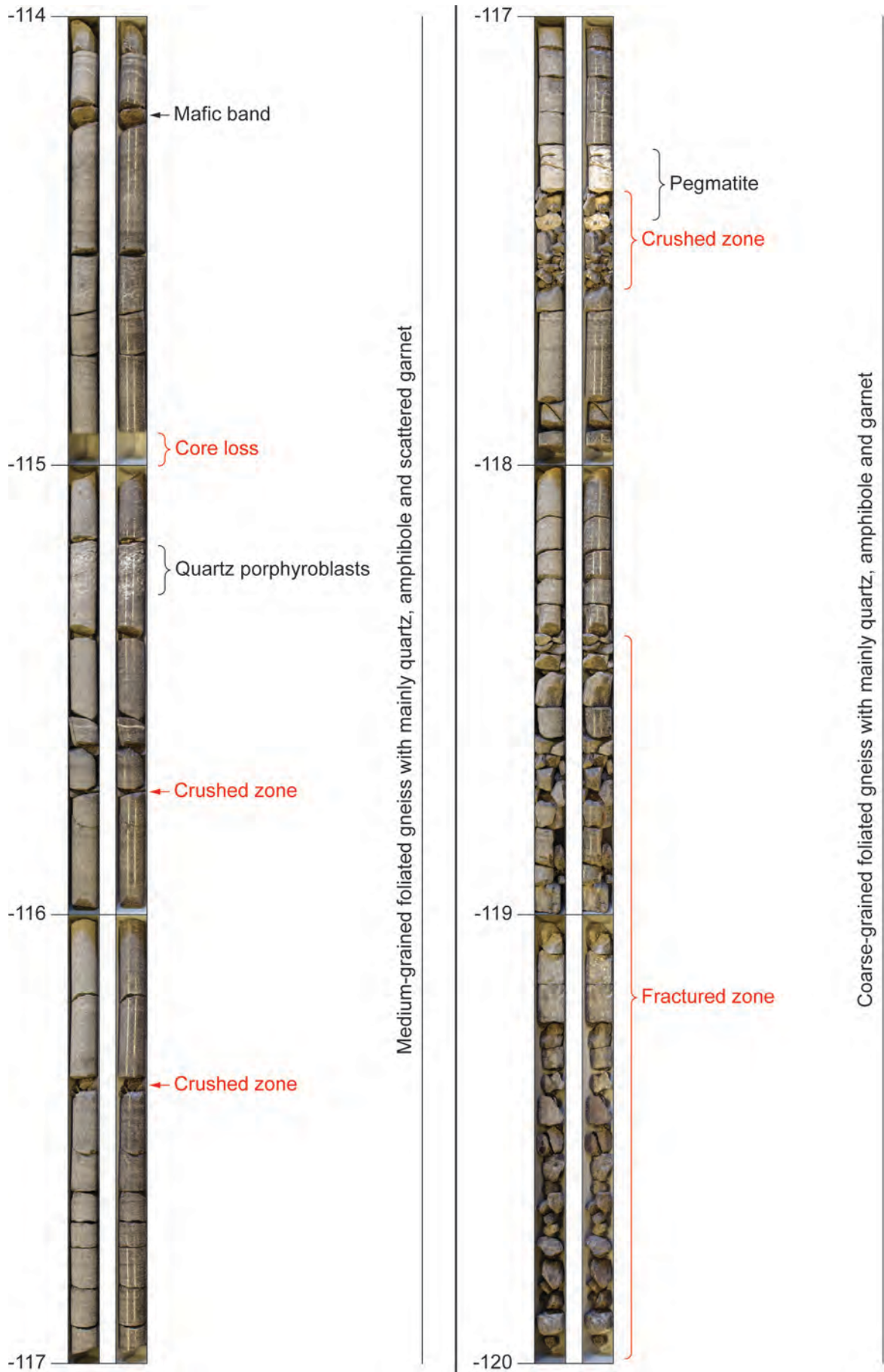


Figure A1.19: Geological and engineering geological core logging from 114 to 120 m depth with pictures of the dry (left) and wet (right) core.

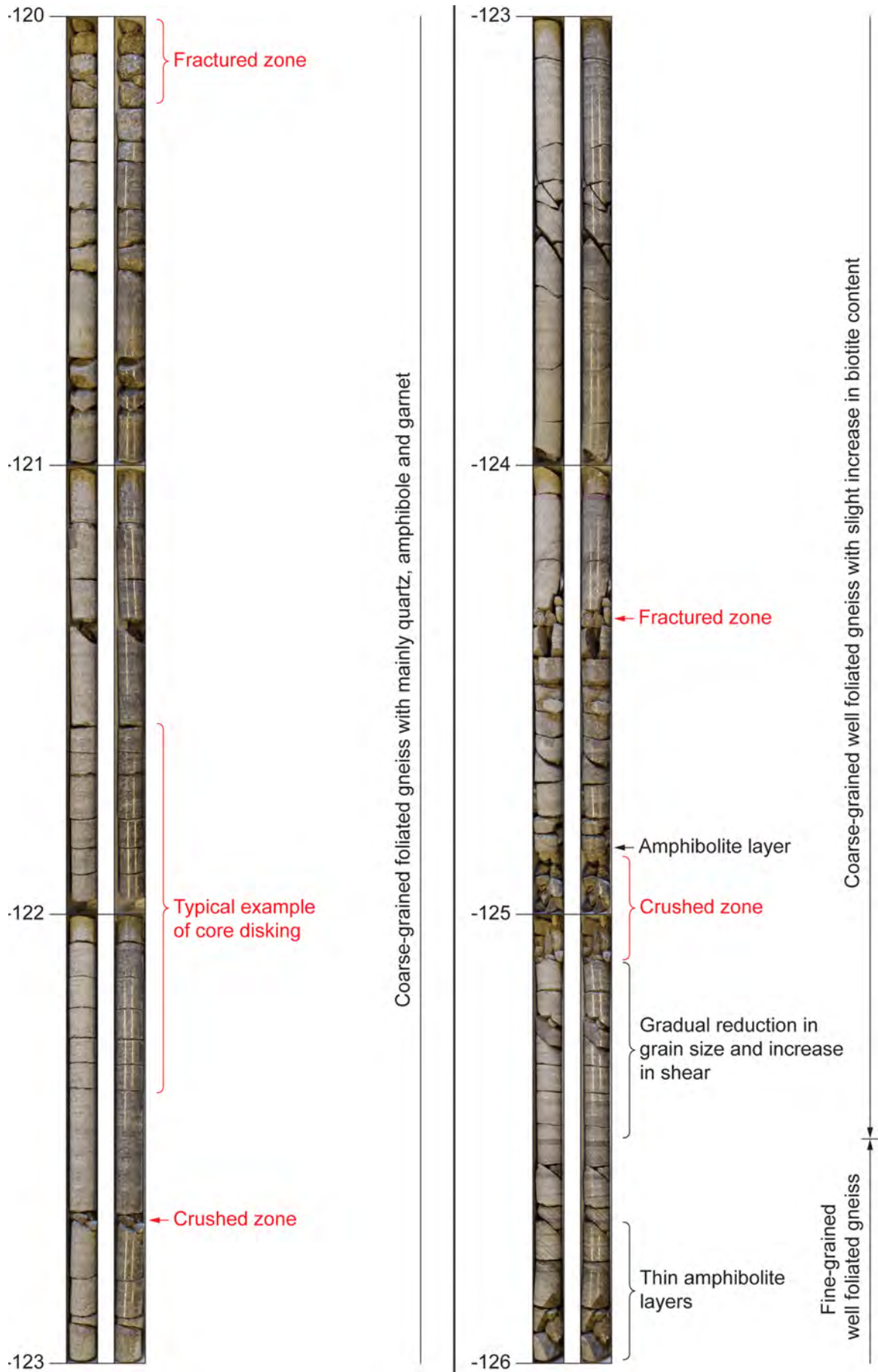


Figure A1.20: Geological and engineering geological core logging from 120 to 126 m depth with pictures of the dry (left) and wet (right) core.

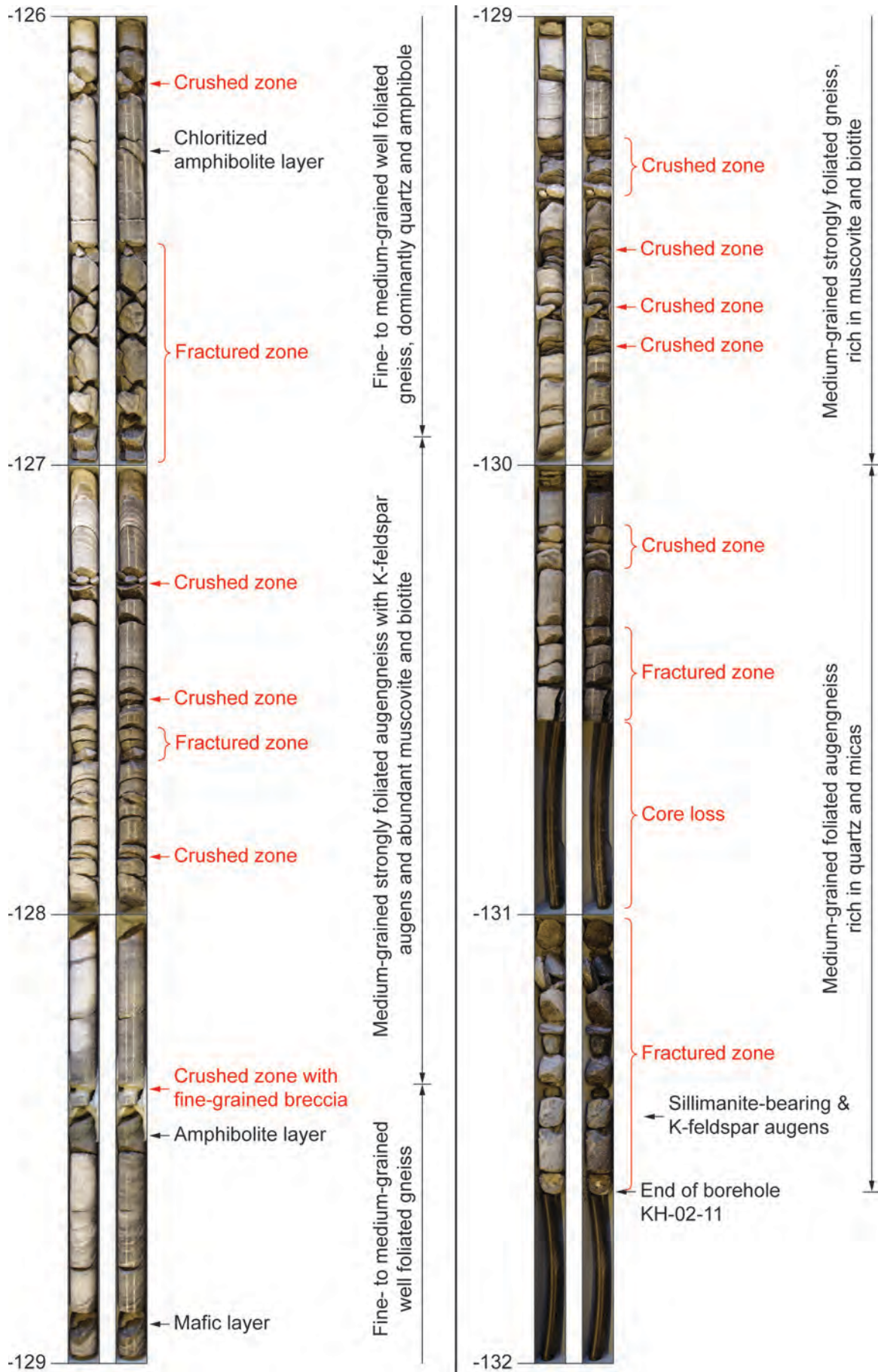


Figure A1.21: Geological and engineering geological core logging from 126 to 131.6 m depth with pictures of the dry (left) and wet (right) core.

Appendix 2: Detailed description of the geological core logging of borehole KH-02-11

The table in Appendix 2 presents the detailed geological description of the core from borehole KH-02-11. The rock types (numbers 1 to 6) refer to the six lithologies described by Saintot et al. (2011) (see also section 2.1).

Depth [m]	Rock type	Description
6–7	3, 2	Fine-grained well foliated gneiss with quartz, plagioclase, amphibole and 1 cm large garnet. At 6.75–7.15 m: amphibolite.
7–8	2, 1, 3	Fine-grained well foliated gneiss. At 7.20–7.36 m: pegmatite with K-Feldspar, quartz, muscovite.
8–9	3, 6	Fine-grained well foliated gneiss. At 8.30–9.00 m: medium-grained augengneiss with K-feldspar and plagioclase augens.
9–10	6	Medium-grained augengneiss with higher content of feldspars, hornblende-bearing, slightly less developed foliation. Porphyroblasts show ductile shear.
10–11	6	Medium-grained augengneiss. At 10.50–10.80 m: coarse-grained augengneiss with predominantly K-feldspar augens, biotite, amphibole and quartz.
11–12	6	Medium-grained augengneiss with 3–5 mm large K-feldspar and plagioclase augens, less developed foliation.
12–13	6	Medium-grained augengneiss with K-feldspar, plagioclase and amphibole. At 12.90–13.00 m: amphibole-rich. Gradual increase in foliation dip angle. Felsic foliation-parallel veins associated with amphibolite.
13–14	6	Medium-grained biotite-rich augengneiss with well developed foliation. At 13.50–14.00 m: foliation dip angle gets subvertical.
14–15	6	Medium-grained weakly foliated augengneiss with centimetric K-feldspar and plagioclase augens displaying sigma shears. Rapid decrease in foliation dip angle.
15–16	6	Medium-grained weakly foliated augengneiss. At 15.20–15.40 m: fractured pegmatite with large muscovite flakes and quartz. At 15.40–16.05 m: coarse-grained weakly foliated augengneiss.
16–17	6	Coarse-grained strongly foliated sillimanite-bearing augengneiss. K-feldspar, plagioclase and quartz augens contained in a fine-grained amphibole-rich matrix.
17–18	6	Coarse-grained strongly foliated sillimanite-bearing augengneiss. Increase in quartz content at 17.90 m. Variably foliated.
18–19	6	Coarse-grained foliated augengneiss with large K-feldspar and plagioclase augens. At 18.50–18.90 m: large augens and poorly developed foliation.
19–20	4	Fine-grained foliated sillimanite-bearing augengneiss with K-feldspar augens. Mafic matrix with biotite and possibly amphibole, banded mineral separation. Steeply-dipping foliation, dextral shear on indicators.
20–21	4	Fine-grained augengneiss with dominantly plagioclase augens showing asymmetric sinistral shear sigma-crystals. Presence of sillimanite stops at 20.35 m.
21–22	4, 3, 4	Fine-grained foliated augengneiss with scattered plagioclase augens. At 21.40–21.60 m: absence of augens. At 21.80–22.00: foliation-parallel felsic veins.
22–23	4, 6	Fine-grained foliated augengneiss with scattered plagioclase augens and fine-grained matrix of biotite, quartz and possible amphibole. At 22.70 m: quartz vein discordant to foliation. At 22.80–23.00: medium-grained strongly foliated augengneiss.
23–24	6, 3	Medium-grained strongly foliated augengneiss with plagioclase, k-feldspar, quartz, biotite and amphibole. Gradual decreasing porphyroblast content towards 23.75 m: fine-grained foliated gneiss. At 23.95–24.25 m: folded amphibolite with retrograde chloritization.
24–25	3	Fine-grained strongly foliated gneiss with scattered plagioclase porphyroblasts.
25–26	3	Fine-grained strongly foliated gneiss with scattered plagioclase porphyroblasts. Vuggy rock at 25.65 m.
26–27	4	Fine-grained well foliated garnet-bearing augengneiss.
27–28	4	Fine-grained well foliated garnet-bearing augengneiss with bands of chloritized amphibolite.
28–29	2	Fine-grained strongly foliated amphibolitic gneiss. Foliation-parallel bands of chloritized amphibolite, altered rims.
29–30	2	Fine-grained strongly foliated amphibolitic gneiss. At 29.70 m: 10 cm large, ductile rotated K-feldspar and plagioclase augens.

Depth [m]	Rock type	Description
30–31	2	Fine-grained foliated amphibolitic gneiss. Less apparent foliation, possibly due to lack of light minerals. At 30.70–30.75 m: felsic vein.
31–32	2	Fine-grained well foliated amphibolitic gneiss with scattered plagioclase porphyroblasts. At 31.56–31.63 m: vuggy rock.
32–33	2	Fine-grained well foliated amphibolitic gneiss with scattered plagioclase porphyroblasts. Quartz and amphibole (up to 20%?) are observed on a fresh fracture.
33–34	2	Fine-grained well foliated amphibolitic gneiss with scattered plagioclase porphyroblasts.
34–35	2, 1	Fine-grained well foliated amphibolitic gneiss until 34.47 m. At 34.47–35.37: Pegmatite with quartz, plagioclase, orthoclase, muscovite, garnet. Cracks occur in muscovite layers. Pegmatite border is foliation-parallel.
35–36	1, 2	Pegmatite with well developed garnets. At 35.37 m: fine-grained foliated amphibolitic gneiss. At 35.73–35.83 m: garnet-bearing pegmatite.
36–37	2	Fine-grained foliated amphibolitic gneiss with predominantly biotite, amphibolite, quartz and plagioclase(?).
37–38	2	Fine-grained foliated amphibolitic gneiss. At 37.25–37.35 m: vuggy rock. At 37.83–38.15 m: crushed rock cemented by driller.
38–39	2	Fine-grained foliated amphibolitic gneiss.
39–40	2	Fine-grained foliated amphibolitic gneiss with some mineralized veins. Foliation is less visible due to lack of light minerals. At 39.67–40.17 m: greenish colour, maybe due to retrograde metamorphism.
40–41	2	Fine-grained foliated amphibolitic gneiss with scattered strongly sheared and elongated porphyroblasts highlighting the foliation.
41–42	2	Fine-grained foliated amphibolitic gneiss. At 41.25 m: felsic ductile deformed porphyroblast.
42–43	2	Fine-grained foliated amphibolitic gneiss. Decrease in felsic minerals, increasing amphibole content, absence of porphyroblasts.
43–44	2, 6	Fine-grained well foliated amphibolitic gneiss. At 43.75 m: gradual transition into coarse-grained well foliated sillimanite-bearing augengneiss with 3–5 mm large K-feldspar augens.
44–45	6	Coarse-grained strongly foliated sillimanite-bearing augengneiss.
45–46	6	Coarse-grained strongly foliated sillimanite-bearing augengneiss with K-feldspar augens, abundant biotite, amphibole, quartz and garnet.
46–47	6	Coarse-grained well foliated sillimanite-bearing augengneiss with 2–5 mm large augens.
47–48	6	Coarse-grained well foliated sillimanite-bearing augengneiss with partly rotated augens and steeply-dipping foliation.
48–49	6	Coarse-grained well foliated sillimanite-bearing augengneiss with subvertical foliation.
49–50	6	Coarse-grained well foliated sillimanite-bearing augengneiss with subvertical foliation. At 49.20 cm: vuggy rock.
50–51	6	Coarse-grained well foliated sillimanite-bearing augengneiss. At 50.35 m: foliation dip angle decreases to moderate.
51–52	6	Coarse-grained well foliated sillimanite-bearing augengneiss.
52–53	6	Coarse-grained well foliated augengneiss with increasing quartz and plagioclase content, absence of sillimanite. At 52.20 m: 10 cm thick amphibolite layer. At 52.50–52.79 m: chlorite-coated fractures.
53–54	6	Coarse-grained well foliated augengneiss. Sigma porphyroblasts indicate dextral shear.
54–55	6	Coarse-grained well foliated augengneiss. At 54.50–55.00 m: increasing K-feldspar content.
55–56	6	Coarse-grained well foliated sillimanite-bearing augengneiss.
56–57	6	Coarse-grained well foliated sillimanite-bearing augengneiss. At 56.80 m: 4 cm thick amphibolite layer.
57–58	6	Coarse-grained well foliated sillimanite-bearing augengneiss. Foliation dip angle decreases. At 57.30 m: strongly foliated with strong elongation of minerals. At 57.85–58.20 m: strong shearing and chloritized amphibolite layers.
58–59	6	Coarse-grained well foliated sillimanite-bearing augengneiss. At 58.60 m: Presence of muscovite, decrease in grain size and gradual transition into fine-grained well foliated muscovite-bearing gneiss.

Depth [m]	Rock type	Description
59–60	3	Fine-grained well foliated muscovite-bearing gneiss. High mica content, absence of sillimanite.
60–61	3	Fine-grained well foliated muscovite-bearing gneiss. Absence of porphyroblasts, steeply-dipping foliation. At 60.95 m: felsic vein discordant to foliation.
61–62	2	Fine-grained foliated amphibolitic gneiss.
62–63	5	Fine-grained foliated amphibolitic gneiss. At 62.17 m: coarse-grained muscovite-bearing gneiss with typical banding (separation between felsic and mafic minerals).
63–64	5	Coarse-grained muscovite-bearing gneiss with typical banding and veins of quartz and plagioclase, abundant biotite, zeolite(?) coating on fractures.
64–65	5	Coarse-grained muscovite-bearing gneiss with typical banding
65–66	5	Coarse-grained muscovite-bearing gneiss with typical banding. At 65.40–65.80 m: reduction in grain size and increase in amphibole content. At 65.80 m: fine-grained foliated amphibolitic gneiss.
66–67	2	Fine-grained foliated amphibolitic gneiss, rich in biotite. At 66.28–66.76 m: crushed zoned with three layers of fine-grained clayey breccia. At 66.76–67.00 m: fine-grained biotite-rich and garnet-bearing gneiss.
67–68	3	Fine-grained biotite-rich and garnet-bearing gneiss. High angle foliation displayed by light minerals. At 67.70–67.80 m: zeolite(?) coating on fracture surfaces. At 67.90 m: Increasing quartz and muscovite content.
68–69	3	Fine-grained well foliated muscovite-bearing gneiss. At 68.35–68.70: scattered K-feldspar augens (3–5 mm large).
69–70	3	Fine-grained well foliated muscovite-bearing and amphibole-rich gneiss
70–71	3	Fine-grained well foliated muscovite-bearing and amphibole-rich gneiss. At 70.25–70.75 m: medium- to coarse-grained zone with high muscovite and quartz content.
71–72	3, 1, 3	Fine-grained well foliated muscovite-bearing and amphibole-rich gneiss. At 71.16–71.71 m: pegmatite with muscovite, garnet, quartz, plagioclase, orthoclase.
72–73	3	Fine-grained well foliated muscovite-bearing gneiss, foliation-parallel veins
73–74	3	Fine-grained well foliated muscovite-bearing gneiss. At 73.65–74.00 m: high content of felsic veins, strongly foliated, muscovite- and biotite-rich.
74–75	3	Fine-grained strongly foliated muscovite-bearing gneiss with high mica content and scattered porphyroblasts, steeply dipping foliation. At 74.14 m: garnet-bearing. At 74.90 m: elongated plagioclase vein.
75–76	3	Fine-grained strongly foliated muscovite-bearing gneiss
76–77	6	Medium-grained strongly foliated augengneiss with K-feldspar augens. At 76.50–76.70 m: plagioclase augens. At 76.70 m: fine-grained well foliated muscovite-bearing gneiss. At 76.85–77.10 m: three chloritized amphibolite layers with tight isoclinal folds.
77–78	3	Fine-grained well foliated muscovite-bearing gneiss with increasing presence of porphyroblasts with depth. At 77.18 m: garnet-bearing.
78–79	6	Medium-grained foliated sillimanite-bearing augengneiss with K-feldspar augens indicating dextral shear. At 78.08 m: foliation-parallel amphibolite layer.
79–80	6, 4	Fine-grained strongly foliated sillimanite-bearing augengneiss with K-feldspar augens.
80–81	4, 3	Fine-grained strongly foliated sillimanite-bearing augengneiss. At 80.30 m: fine-grained strongly foliated gneiss with typical banding, absence of sillimanite. At 80.65–80.70 m: plagioclase and K-feldspar bands.
81–82	3	Fine-grained strongly foliated gneiss with typical banding. At 81.05 m: chloritized amphibolite layer. At 81.55–82.00 m: increasing muscovite, biotite and amphibole content.
82–83	3, 6	Fine-grained strongly foliated gneiss with non-foliated quartz veins. At 82.40 m: medium-grained foliated muscovite-bearing augengneiss with K-feldspar augens.
83–84	3	Medium-grained foliated muscovite-bearing augengneiss. At 83.30 m: fine-grained strongly foliated muscovite- and biotite-rich gneiss with few porphyroblasts, highly strained, steeply-dipping foliation.
84–85	5	Medium-grained well foliated muscovite- and biotite-rich gneiss. Low rock strength (peels of in foliation-parallel disks under finger pressure). At 84.75–84.86 m: fine-grained clayey breccia.
85–86	5	Fine-grained well foliated muscovite-rich gneiss, absence of porphyroblasts. More competent rock mass.

Depth [m]	Rock type	Description
86–87	3, 1	Fine- to medium-grained well foliated muscovite-rich gneiss with dominantly quartz and biotite. At 86.57 m: 2 cm thick biotite layer. At 86.72 m: garnet-bearing. At 86.80: pegmatite.
87–88	1	Pegmatite with well developed quartz and K-feldspar phenocrysts and up to 7–8 mm large muscovite flakes, garnet-bearing. Muscovite mineral orientation produces a well defined, but weak foliation.
88–89	1	Garnet-bearing pegmatite.
89–90	1	Garnet-bearing pegmatite with large aggregates of quartz and K-feldspar. At 89.33–89.90 m: absence of K-feldspar.
90–91	1, 3	Garnet-bearing pegmatite with high mica content. At 90.45 m: fine-grained strongly foliated mica-rich gneiss.
91–92	3	Fine-grained strongly foliated mica-rich gneiss with increasing amphibole content. At 91.47 m: 5 cm thick pegmatite layer.
92–93	3	Fine-grained strongly foliated mica-rich gneiss.
93–94	3	Fine-grained strongly foliated mica-rich gneiss with several chloritized amphibolite bands (at 93.02, 93.15, 93.25, 93.34, 93.40, 93.45, 93.51 and 93.78 m). At 93.15 m: foliation-parallel fracture surface with mineral lineation indicating dextral oblique down-dip movement. At 93.60–93.85 m: vuggy rock.
94–95	3, 2	Fine-grained strongly foliated mica-rich gneiss with chloritized amphibolite bands at 94.20–94.40 m. At 94.65 m: fine-grained foliated amphibolitic gneiss. At 94.60–94.95 m: vuggy rock.
95–96	2	Fine-grained foliated amphibolitic gneiss. At 95.12 m: vuggy rock. At 95.37 m: muscovite layer. At 95.58–95.60 m: fine-grained clayey breccia, green coloured.
96–97	3	Fine- to medium-grained strongly foliated mica-rich gneiss with several chloritized amphibolite bands (at 96.30, 96.55 and 96.90 m). At 96.46 m: zone with plagioclase sigma crystals. At 96.60 m: malachite aggregate in fracture.
97–98	3	Fine- to medium-grained strongly foliated mica-rich gneiss with several chloritized amphibolite bands (at 97.57–97.67 (vuggy), 97.71–97.80 and 97.86–97.95 m (vuggy)), steeply-dipping foliation.
98–99	3	Fine- to medium-grained strongly foliated mica-rich gneiss with several chloritized amphibolite bands (at 98.00–98.33 and 98.47–99.00 m), steeply-dipping foliation. Vuggy rock at 98.10, 98.20 and 98.82 m.
99–100	3	Fine- to medium-grained strongly foliated mica-rich gneiss with several chloritized amphibolite bands (at 99.10–99.15, 99.35–99.55 and 99.60–99.75 m (vuggy)), garnet-bearing.
100–101	3	Fine- to medium-grained strongly foliated mica-rich gneiss with several chloritized amphibolite bands (at 100.19 and 100.70–100.80 m). Vuggy rock at 100.06, 100.23, 100.53, 100.73–100.78 m. At 100.73 m: garnet-bearing.
101–102	3	Fine- to medium-grained strongly foliated mica-rich gneiss with several chloritized amphibolite bands (at 101.10–101.15, 101.22–101.45 (vuggy) and 101.70–101.83 m (vuggy)).
102–103	4	Fine-grained strongly foliated garnet-bearing augengneiss with 1–2 mm large augens. Dextral shear indications on clasts. At 102.62 m: vuggy amphibolite band.
103–104	4	Fine-grained strongly foliated garnet-bearing augengneiss with 2–5 mm large augens. At 103.41–103.63 m: sillimanite-bearing associated to K-feldspar augens. At 103.63–104.00 m: plagioclase augens, decrease in size of porphyroblasts.
104–105	3	Fine-grained strongly foliated gneiss with dominantly quartz, biotite and amphibole.
105–106	3	Fine-grained well foliated gneiss. At 105.15 m: garnet-bearing. At 105.30 m: chlorite-coating on fracture surface.
106–107	3	Fine-grained well foliated gneiss with dominantly quartz and amphibole.
107–108	3	Fine-grained well foliated gneiss with dominantly quartz and amphibole. At 107.48 m: isoclinal fold.
108–109	3	Fine-grained well foliated gneiss with dominantly quartz and amphibole. At 108.92–109.10 m: pegmatite layer with coarse-grained plagioclase, quartz, amphibole and garnet. Pegmatite is discordant to foliation in gneiss.
109–110	3	Fine-grained well foliated gneiss with dominantly quartz and amphibole. At 109.90 m: scattered quartz and plagioclase porphyroblasts

Depth [m]	Rock type	Description
110–111	3	Fine-grained well foliated gneiss with scattered 3–4 mm large quartz and plagioclase porphyroblasts. Presence of porphyroblasts may indicate a reduction in strain.
111–112	3	Fine-grained weakly foliated gneiss with dominantly quartz and amphibole. At 111.05 m: quartz band.
112–113	3	Fine-grained weakly foliated gneiss with dominantly quartz and amphibole. At 112.23 m: quartz band.
113–114	3, 5	Fine-grained weakly foliated gneiss with scattered 1–2 mm large quartz aggregates. At 113.60 m: increase in grain size to medium-grained well foliated gneiss.
114–115	5	Medium-grained well foliated gneiss with dominantly quartz, amphibole and scattered garnet. At 114.20 m: mafic band.
115–116	5	Medium-grained well foliated gneiss. At 115.20–115.30 m: zone with quartz porphyroblasts indicating possibly dextral shear.
116–117	5	Medium-grained well foliated gneiss, scattered garnets
117–118	5	Coarse-grained foliated gneiss. At 117.30–117.45 m: pegmatite with aggregates of quartz, feldspar and hornblende.
118–119	5	Coarse-grained foliated gneiss with dominantly quartz and amphibole. Increase in garnet content.
119–120	5	Coarse-grained foliated gneiss.
120–121	5	Coarse-grained foliated gneiss with up to 3 mm large garnets.
121–122	5	Coarse-grained foliated gneiss.
122–123	5	Coarse-grained foliated gneiss.
123–124	5	Coarse-grained well foliated gneiss, slight increase in biotite content.
124–125	5	Coarse-grained well foliated biotite-bearing gneiss. At 124.85 m: 1 cm thick amphibolite layer.
125–126	5, 3	Coarse-grained well foliated biotite-bearing gneiss, gradual reduction in grain size towards 125.50 m. Increase in shear interpreted from increased elongation of quartz. At 125.50 m: fine-grained strongly foliated gneiss with scattered garnets. At 125.70–126.00 m: several thin amphibolite layers with quartz rim.
126–127	3	Fine- to medium-grained well foliated gneiss, rich in quartz and amphibole. At 126.30 m: chloritized amphibolite layer. Increase of K-feldspar porphyroblasts and biotite content towards 127.00 m.
127–128	6	Medium-grained strongly foliated sillimanite-bearing augengneiss with 2–5 mm large K-feldspar augens, abundant biotite and muscovite.
128–129	6, 5	Medium-grained strongly foliated sillimanite-bearing augengneiss. At 128.35–128.50 m: Crushed zone with fine-grained breccia within amphibolite layer. At 128.50 m: Fine- to medium-grained well foliated gneiss, absence of sillimanite. At 128.95 m: mafic layer.
129–130	5	Medium-grained strongly foliated gneiss, rich in muscovite and biotite, absence of sillimanite.
130–131	6	Medium-grained foliated augengneiss with dominantly quartz and micas.
131–131.6	6	Medium-grained foliated augengneiss with dominantly quartz and micas.



Norges geologiske undersøkelse
Postboks 6315, Sluppen
7491 Trondheim, Norge

Besøksadresse
Leiv Eirikssons vei 39, 7040 Trondheim

Telefon 73 90 40 00
Telefax 73 92 16 20
E-post ngu@ngu.no
Nettside www.ngu.no

*Geological Survey of Norway
PO Box 6315, Sluppen
7491 Trondheim, Norway*

*Visitor address
Leiv Eirikssons vei 39, 7040 Trondheim*

*Tel (+ 47) 73 90 40 00
Fax (+ 47) 73 92 16 20
E-mail ngu@ngu.no
Web www.ngu.no/en-gb/*